© 2016. Published by The Company of Biologists Ltd | Development (2016) 143, 2983-2993 doi:10.1242/dev.134403

RESEARCH ARTICLE

Wallenda/DLK protein levels are temporally downregulated by Tramtrack69 to allow R7 growth cones to become stationary boutons

Alexander I. Feoktistov and Tory G. Herman*

ABSTRACT

Dual leucine zipper kinase (DLK) promotes growth cone motility and must be restrained to ensure normal development. PHR (Pam/Highwire/RPM-1) ubiquitin ligases therefore target DLK for degradation unless axon injury occurs. Overall DLK levels decrease during development, but how DLK levels are regulated within a developing growth cone has not been examined. We analyzed the expression of the fly DLK Wallenda (Wnd) in R7 photoreceptor growth cones as they halt at their targets and become presynaptic boutons. We found that Wnd protein levels are repressed by the PHR protein Highwire (Hiw) during R7 growth cone halting, as has been observed in other systems. However, as R7 growth cones become boutons, Wnd levels are further repressed by a temporally expressed transcription factor, Tramtrack69 (Ttk69). Previously unobserved negative feedback from JNK also contributes to Wnd repression at both time points. We conclude that neurons deploy additional mechanisms to downregulate DLK as they form stable, synaptic connections. We use live imaging to probe the effects of Wnd and Ttk69 on R7 bouton development and conclude that Ttk69 coordinates multiple regulators of this process.

KEY WORDS: DLK, Wallenda, Tramtrack69, JNK, R7, *Drosophila*

INTRODUCTION

The pattern of connectivity among neurons depends upon the behavior of growth cones, motile structures at the tips of axons. Growth cones extend, turn, pause and retract as they navigate specific pathways, halt upon contacting the appropriate target cells, and ultimately become stationary presynaptic boutons. Although much of this behavior is regulated by extrinsic cues (Lowery and Van Vactor, 2009; Vitriol and Zheng, 2012), cell-intrinsic factors also play a crucial role in regulating the growth cone cytoskeleton (Goldberg, 2004; Moore and Goldberg, 2011; Mar et al., 2014; Steketee et al., 2014). In particular, dual leucine zipper kinase (DLK), a mitogen-activated protein kinase kinase kinase (MAP3K), is a potent cell-intrinsic regulator of microtubule dynamics. DLK levels increase in response to axon injury and promote growth cone assembly and extension by activating the MAPKs JNK and p38 (Nakata et al., 2005; Collins et al., 2006; Hirai et al., 2006; Lewcock et al., 2007; Eto et al., 2010; Xiong et al., 2010; Nix et al., 2011; Klinedinst et al., 2013). Although loss of DLK has only subtle effects on normal development (Collins et al., 2006; Fernandes et al., 2014; Shin and DiAntonio, 2011; Wang et al., 2013), DLK overexpression cell-autonomously disrupts axon connectivity by causing growth cones to extend beyond their targets (Lewcock, et al., 2007; Wang et al., 2013; Baker et al., 2014; Opperman and Grill, 2014). DLK activity is therefore normally limited by PHR family E3 ubiquitin ligases, which target DLK for degradation in the absence of injury (Liao et al., 2004; Nakata et al., 2005; Collins et al., 2006; Wu et al., 2007; Brace et al., 2014). DLK levels have been reported to decrease during development (Collins et al., 2006; Eto et al., 2010), suggesting that PHR or other mechanisms progressively downregulate DLK as neurons form stable connections. However, this has not been tested.

To test whether DLK is indeed temporally regulated in growth cones, we studied the R7 photoreceptor neurons in the *Drosophila* eye. R7 growth cone motility decreases in two main phases (Ting et al., 2005; Kniss et al., 2013; Chen et al., 2014; Özel et al., 2015): (1) after extending from the retina, R7 growth cones halt within a specific layer in the medulla but remain expanded with multiple dynamic processes; and (2) as the R7 axons lengthen by passive stretch growth, their growth cones gradually decrease in volume, their processes decrease in number and motility, and they ultimately become smooth, stationary boutons. We expected that the *Drosophila* DLK Wnd would be repressed by the PHR Hiw during halting (phase 1), as in other systems, but wondered whether Wnd is then further downregulated to allow development into boutons (phase 2) to occur.

Here, we show that, as expected, R7 growth cones require Hiw during phase 1 to repress and thereby prevent Wnd from disrupting R7 growth cone halting. However, we find that Hiw is not required during phase 2. Instead, a transcription factor, Ttk69 (Ttk – FlyBase), that is specifically expressed during phase 2 (Kniss et al., 2013) acts redundantly with Hiw to ensure that Wnd levels remain low as R7 growth cones become boutons. In contrast to the JNK-dependent positive feedback that has been observed during axon injury in mammalian cell culture (Huntwork-Rodriguez et al., 2013), we show that during both phases of R7 development, Wnd protein levels are repressed by JNK-dependent negative feedback. Finally, we use live imaging to show that Wnd overexpression and Ttk69 loss have overlapping but distinct effects on the behavior of R7 growth cones as they become presynaptic boutons. We conclude that neurons can use temporal factors in addition to Hiw to increase the repression of Wnd as their connections become more stable, and that in R7s the temporal factor Ttk69 promotes the development of growth cones into boutons by repressing multiple regulators of growth cone dynamics.

RESULTS

Wnd protein is downregulated independently of Hiw in R7 growth cones as they become presynaptic boutons

Previous work has shown that average levels of DLK decrease during development (Collins et al., 2006). One possibility is that

Institute of Molecular Biology, Department of Biology, University of Oregon, Eugene, OR 97403, USA.

*Author for correspondence (herman@uoregon.edu)

A.I.F., 0000-0001-6597-981X; T.G.H., 0000-0002-7686-4986

Received 22 December 2015; Accepted 23 June 2016

Development (2016) 143, 2983-2993 doi:10.1242/dev.134403

individual neurons progressively downregulate DLK as their growth cones lose motility. To test this, we examined Wnd levels in R7 growth cones. We anticipated that, as in other systems, R7 growth cones would use Hiw to repress Wnd as they halt at their target layer [24 h after puparium formation (h APF)]. However, we wanted to know whether Wnd is repressed further in R7 growth cones as they become stationary boutons (60 h APF). We therefore used anti-Wnd antibodies to quantify Wnd levels in R7 growth cones at these time points; we were unable to analyze actively extending R7 growth cones because of their location and orientation. At 24 h APF, we found that anti-Wnd staining in wild-type R7 growth cones is indistinguishable from that in *wnd* mutants (Fig. 1A,A′,E; Fig. S1D,D′), which have previously been shown to be protein null (Wu et al., 2007), but that loss of *hiw* increases Wnd levels significantly (Fig. 1B,B′,E). We conclude that, as expected, Hiw is required to repress Wnd during R7 growth cone halting.

At 60 h APF, anti-Wnd staining in wild-type R7 growth cones is again low and indistinguishable from that in *wnd* mutants (Fig. 1C,C′,E); any potential decrease from 24 h APF levels is therefore below our level of detection. However, loss of *hiw* causes a much smaller increase in Wnd (Fig. 1D,D′,E). Wnd levels therefore decrease significantly in *hiw* mutant R7 growth cones between 24 and 60 h APF. We conclude that Wnd is downregulated by a Hiw-independent mechanism as R7 growth cones become boutons.

During R7 growth cone halting, Wnd must be repressed by Hiw to prevent extension beyond the correct target layer

We next compared the effects of increased Wnd during halting and bouton development. We anticipated that, as in other systems, increased Wnd during halting might cause R7 growth cones to project beyond their normal target layer (Schaefer et al., 2000; Lewcock et al., 2007; Yan et al., 2009; Wang et al., 2013; Baker et al., 2014; Opperman and Grill, 2014). We used either the photoreceptor-specific *chaoptin-Gal4* (*chp-Gal4*; Fig. 2A-D′) or the R7-specific *PM181-Gal4* (Fig. S2A-B″) driving *UAS-mCD8-GFP* to label R7 axons in wild-type and *hiw* mutant brains at 24 h APF. We found that R7 growth cones in *hiw* mutants halt at the correct target layer but are abnormally elongated (a hallmark of forward-moving growth cones; Godement et al., 1994) and frequently extend long, thin processes beyond their targets (Fig. 2B, B′,E,F; Fig. S2B-B″). Because PHR proteins can have DLK-independent effects (Burgess et al., 2004; D'Souza et al., 2005; McCabe et al., 2004; Collins et al., 2006; Bloom et al., 2007; Grill et al., 2007; Li et al., 2008; Brace et al., 2014), we verified that the upregulation of Wnd in *hiw* mutants is responsible for disrupting R7 growth cone halting: loss of *wnd* from *hiw* mutants fully rescues the overextensions (Fig. 2C-F), and using *chp-Gal4* to overexpress Wnd in wild-type R7s is sufficient to cause overextensions (Fig. 2G; Fig. S2E,E′). We conclude that Hiw is required to repress Wnd in R7 growth cones to promote normal halting. As in other systems (Collins et al., 2006; Fernandes et al., 2014; Shin and DiAntonio, 2011; Wang et al., 2013), loss of *wnd* does not disrupt R7 growth cone morphology or connectivity (Fig. 2C,C′,E,F; data not shown).

During R7 growth cone halting, Wnd is also repressed by negative feedback from JNK

To test whether Wnd disrupts R7 halting by acting upstream of JNK (Bsk – FlyBase) (Hirai et al., 2002; Collins et al., 2006; Eto et al., 2010; Yan and Jin, 2012), we co-expressed Wnd with a dominant-negative version of JNK (JNK^{DN}; Weber et al., 2000). We found that JNK^{DN} almost completely eliminates the processes that Wnd-overexpressing R7 growth cones extend (Fig. 2G; Fig. S2F,F′),

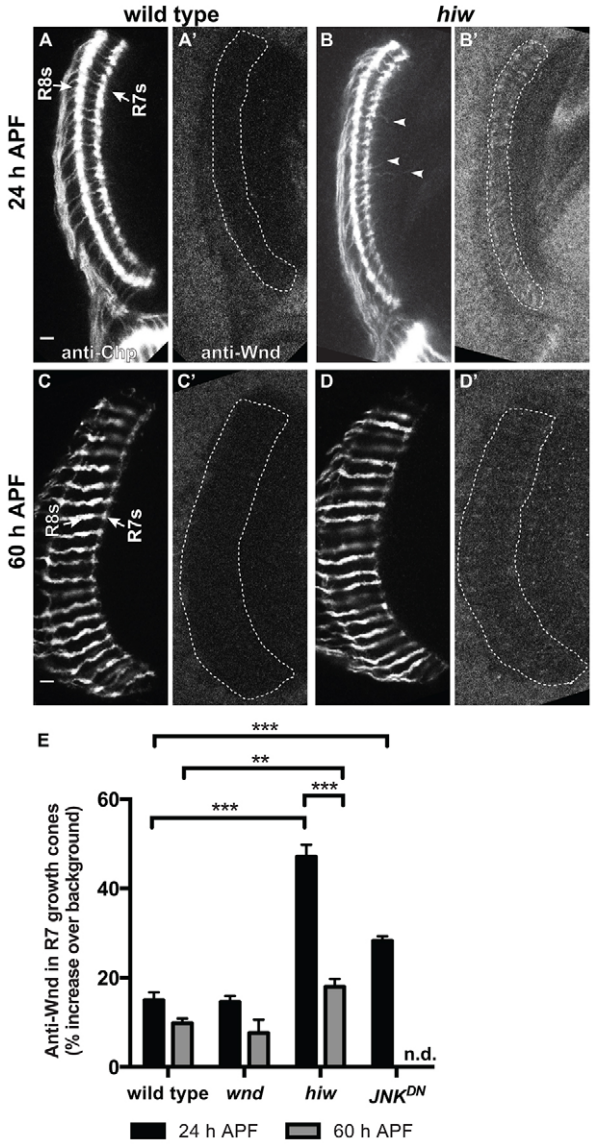

Fig. 1. Wnd protein is downregulated independently of Hiw in R7 growth cones as they become presynaptic boutons. (A-D′) Pupal medullas (29°C) in which R7 and R8 axons are labeled with anti-Chp (A-D) and anti-Wnd (A′-D′). Arrows in A indicate the R7 and R8 target layers. (E) Quantification of anti-Wnd levels in R7 growth cones (for details see Materials and Methods). At 24 h APF, wild-type R7 growth cones (A,A′) have halted at their medullar target layer but remain expanded. *hiw* mutant R7 growth cones (B,B′) contain significantly more anti-Wnd staining (E) and extend processes beyond their target layer (arrowheads). We note that loss of Hiw also increases anti-Wnd staining in R8 growth cones at this time (Fig. 1A-B′; data not shown). However, by 60 h APF, *hiw* mutant R7 growth cones are indistinguishable from wild type and contain significantly less anti-Wnd staining than at 24 h APF (C-E). The level of anti-Wnd staining in wild-type R7 growth cones is indistinguishable from that in *wnd* deletion mutants at each time point, indicating that R7 growth cones normally express little or no Wnd protein during both halting and bouton development. Using *chp-Gal4* to drive expression of dominant-negative JNK (JNK^{DN}) in R7s also significantly increases anti-Wnd staining in their growth cones at 24 h APF, indicating that JNK provides negative feedback to Wnd (see Fig. 2). Error bars represent s.e.m. $^{**}P<0.001$, $^{***}P<0.0001$ based on two-tailed *t*-tests. n=14, 16, 5, 6, 10, 17 and 8 brains, from left to right on the graph. n.d., no data. Scale bars: 5 µm.

indicating that Wnd acts upstream of JNK in this process. However, we also noticed that expressing JNK^{DN} in R7s significantly increases Wnd levels in R7 growth cones (Fig. 1E). Consistent

Development (2016) 143, 2983-2993 doi:10.1242/dev.134403

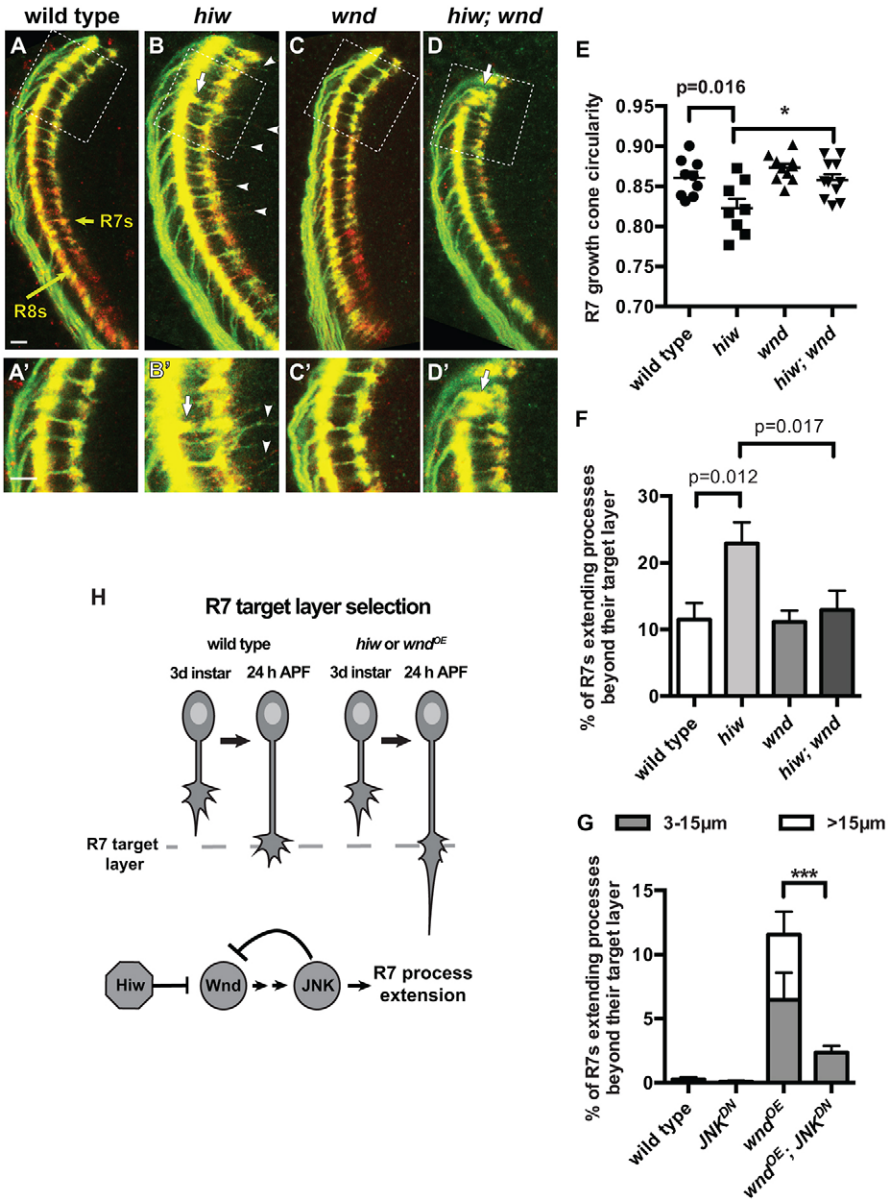

Fig. 2. R7 growth cones require Hiw to repress Wnd as they halt at their target layer. (A-D′) Pupal medullas (24 h APF; 25°C) in which R7 and R8 axons are labeled with *chp-Gal4, UAS-mCD8-GFP* (green) and anti-Chp (red). A′-D′ are enlargements of the boxed regions in A-D with enhanced brightness. Yellow arrows in A indicate the R7 and R8 target layers. (E-G) Quantifications of R7 growth cone phenotypes. *hiw* mutant R7 growth cones are elongated (B,B′,E; two-tailed *t*-test) and extend processes beyond their target layer (arrowheads; processes of at least 3 µm are quantified in F; two-tailed *t*-test). R8 growth cones occasionally terminate between the R8 and R7 target layers (arrows in B,B′; 1.7±0.6% versus <0.08% in wild type; Fig. S2B,B′). Loss of *wnd* has no effect on wild-type R7 growth cones (C,C′,E,F) but restores the morphology of *hiw* mutant R7 growth cones to that of wild type (D-F; one-tailed *t*-tests, **P*<0.01). R8 growth cones also occasionally extend beyond their target layer in both *wnd* (data not shown) and *hiw; wnd* mutants (arrows in D,D′). (G) Using *chp-Gal4* to drive co-expression of Wnd (wnd^{OE}) and RFP (as a control for *UAS* copy number) is sufficient to disrupt R7 growth cone halting. Co-expressing Wnd with JNK^{DN} ameliorates this defect (G; ****P*<0.0001; Fig. S2). Error bars represent s.e.m. *n*=9, 8, 11 and 11 brains, from left to right on the graphs in E,F and 7, 8, 7 and 12 from left to right on the graph in G. Scale bars: 5 µm. (H) Model summarizing the roles of Hiw, Wnd and JNK as R7 growth cones halt at their target layer.

with our finding that Wnd requires JNK to disrupt R7 growth cone halting, JNK^{DN} does not disrupt R7 growth cone halting, despite the increased Wnd (Fig. S2D,D′). We conclude that during R7 growth cone halting, JNK acts in a negative-feedback loop that contributes to restricting Wnd levels (Fig. 2H). Mammalian JNK acts in a positive-feedback loop to increase DLK levels during axon regeneration (Huntwork-Rodriguez et al., 2013). However, JNK-mediated negative feedback has not previously been reported.

As R7 growth cones become boutons, Wnd must be repressed to prevent a different defect: lateral extension within their target layer

We next examined the effects of increased Wnd during phase 2 of R7 growth cone development. We again used the *chp* promoter driving GFP expression to label R7 and R8 axons and examined two later time points that span R7 bouton development: (1) 40 h APF, when wild-type R7 axon terminals start assembling active zones but are still expanded and extend multiple thin processes; and (2) 60 h APF, by which time R7 terminals have many active zones, are condensed, and extend fewer processes (Ting et al., 2005; Chen et al., 2014; Özel et al., 2015; see below). We hypothesized that the early defect in R7 growth cone halting caused by *hiw* loss might simply persist or worsen at these time points. However, we found instead that R7 axon terminals in *hiw* mutants are indistinguishable from wild type at both 40 and 60 h APF (Fig. 3A,B,D,E,G,H). We conclude that, despite the modestly increased Wnd levels that persist in older *hiw* mutant R7 growth cones, the earlier effects on R7 growth cone morphology are somehow later corrected, and R7 growth cones develop into morphologically normal boutons.

One possibility is that older R7 growth cones simply become insensitive to increased Wnd levels. Alternatively, the Hiw-independent decrease in Wnd levels that we observed between halting (24 h APF) and bouton development (60 h APF) might allow R7 growth cones to become boutons. To distinguish between these, we used *chp-Gal4* to drive increased expression of Wnd in wild-type R7 neurons – the same manipulation that disrupts R7 growth cone halting at 24 h APF (Fig. 2G; Fig. S2E,E′). We found that despite the prolonged high Wnd levels, the R7 growth cone halting defect is substantially corrected by 48 h APF: only 1.6±0.71% of R7 axon terminals extend processes beyond their target layer at this time point

Development (2016) 143, 2983-2993 doi:10.1242/dev.134403

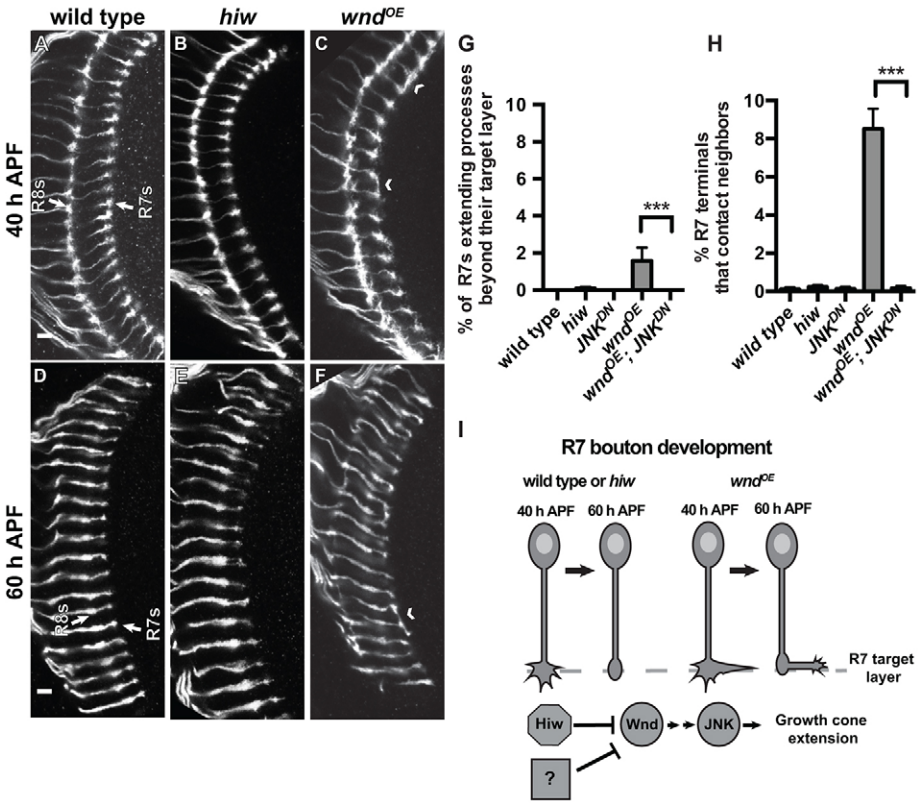

Fig. 3. R7 growth cones do not require Hiw as they become presynaptic boutons, yet Wnd overexpression disrupts this process. (A-F) Pupal medullas (25°C) in which R7 and R8 axons are labeled with *chp-Gal4, UAS-EB1-GFP* (white). Arrows indicate the R7 and R8 target layers. (G,H) Quantification of R7 growth cone phenotypes at 48 h APF (29°C). By 40 h APF (A,B), wild-type and *hiw* mutant R7 axon terminals are indistinguishable. The same is true at 60 h APF (D,E). By contrast, using *chp-Gal4* to drive co-expression of Wnd and control RFP causes R7 axon terminals to contact adjacent R7 terminals (chevrons; quantified in H) and, occasionally, extend processes beyond their target layer (quantified in G). These defects are eliminated by co-expressing Wnd with JNK^{DN} (G,H; ***P<0.0001). Error bars represent s.e.m. n=8, 7, 11, 7 and 10 brains from left to right on graphs. Scale bars: 5 µm. (I) Model summarizing the roles of Hiw, Wnd and JNK as R7 growth cones become stationary boutons.

(Fig. 3C,G) compared with 11.6±2.2% at 24 h APF (P<0.001). However, a significant number of R7 axon terminals at 48 and 60 h APF instead extend laterally and contact adjacent neighbors (Fig. 3C,H). Co-expressing JNK^{DN} together with Wnd completely ameliorates both defects (Fig. 3G,H). We conclude that older R7s are sensitive to increased Wnd, suggesting that the Hiw-independent mechanism that contributes to repression of Wnd during bouton development serves a protective purpose (Fig. 3I). Although the bouton defect caused by increased Wnd is different from the earlier halting defect, Wnd acts through JNK in each case.

Wnd overexpression and Ttk69 loss cause similar defects in R7 bouton development

We previously found that the transcriptional repressor Ttk69 is specifically expressed in R7s after their growth cones halt and is required to prevent a defect in R7 bouton development similar to that caused by Wnd overexpression (Kniss et al., 2013). To compare directly the effects of Wnd and Ttk69 on R7 growth cones, we used *GMR-FLP*/MARCM to generate individual GFP-labeled R7s that were wild type (Fig. 4A,E,H), wild type but overexpressing Wnd (Fig. 4B,C,F,I), or *ttk69* mutant (Fig. 4D,G,J). Consistent with our previous results, individual R7s overexpressing Wnd at 24 h APF have elongated growth cones that extend processes beyond their target layer (Fig. 4B); in addition, some are expanded laterally (Fig. 4C), a defect that was obscured when all R7 growth cones were labeled. At this early time point, Ttk69 is not yet expressed in R7s and *ttk69* mutant R7 growth cones are normal (Kniss et al., 2013; Fig. 4D). By 48 and 60 h APF, R7s overexpressing Wnd frequently extend laterally, causing overlap with neighboring wild-type R7 terminals (Fig. 4F,I); some also extend branches within the M1 layer (data not shown). These defects resemble those caused by Ttk69 loss (Fig. 4G,J), although Ttk69 loss additionally causes some branching in the M3 layer (Fig. 4J). We conclude that Wnd acts cell-autonomously to disrupt R7 growth cone morphology and that Wnd gain and Ttk69 loss cause similar defects in bouton morphology. To assess synapse assembly within these boutons, we used the STaR technique (synaptic tagging with recombination; Chen et al., 2014) to label the active zone component Bruchpilot (Brp). We found that Brp puncta in R7s overexpressing Wnd or *ttk* RNAi are concentrated within the M6 layer as in wild type (Fig. 4K,K′; data not shown; Chen et al., 2014), and also localize to the lateral extensions that occur within M6 (Fig. 4K,K′; data not shown). By contrast, Brp puncta are largely absent from the few forward-projecting processes that persist in older R7s overexpressing Wnd (Fig. 4L,L′). We conclude that Wnd gain and Ttk69 loss do not prevent the abnormal R7 boutons from assembling Brp puncta in the correct layer.

Ttk69 acts in parallel with Hiw and JNK to decrease Wnd protein levels in R7 axon terminals as they become boutons

Because of the similarity of the R7 bouton defects caused by Wnd overexpression and Ttk69 loss, we next tested whether Ttk69 might be responsible for the Hiw-independent repression of Wnd during this process. We found that disrupting Ttk69 does not significantly increase Wnd levels at 48 or 60 h APF (Fig. 5A). However, simultaneous loss of Hiw and Ttk69 in R7s causes a striking increase in Wnd, well beyond the sum of that caused by loss of either alone (Fig. 5A). We conclude that Hiw and Ttk69 act redundantly in R7s to keep Wnd repressed as their growth cones become boutons (Fig. 5C).

We next tested whether JNK represses Wnd during bouton development, as it does during halting. Disrupting JNK in R7s does not increase Wnd levels at 48 h APF (Fig. 5A). However, simultaneous disruption of JNK and Ttk69, like simultaneous disruption of Hiw and Ttk69, causes a significantly greater-than-additive increase in Wnd levels in R7 axon terminals (Fig. 5A). We

Development (2016) 143, 2983-2993 doi:10.1242/dev.134403

conclude that JNK continues to act in a negative-feedback loop to restrict Wnd levels in R7 terminals during bouton development but, like Hiw, is redundant with Ttk69 during this process (Fig. 5C).

To test whether Ttk69, a transcriptional repressor, might directly regulate *wnd* transcription, we used qRT-PCR to quantify the levels of *wnd* mRNA in wild-type retinas and in retinas in which all R neurons expressed *ttk* RNAi. We found no difference, despite being able to detect a significant difference between the wild-type retinas and retinas in which R neurons overexpressed *wnd* (Fig. 5B). We also found that wild-type *wnd* mRNA levels do not detectably decrease between 30 and 48 h APF (Fig. S3A). We conclude that Ttk69 is unlikely to repress Wnd transcriptionally, although there may instead be R7-specific differences in *wnd* mRNA levels that we were unable to detect. We examined whether Ttk69 might regulate levels of *fat facets* mRNA, which encodes a deubiquitinase that acts in parallel with Hiw to regulate Wnd stability, but again found no difference (Fig. S3B). We conclude that Ttk69 acts in parallel with Hiw but upstream of an unknown factor to repress Wnd in R7 growth cones as they become boutons (Fig. 5C).

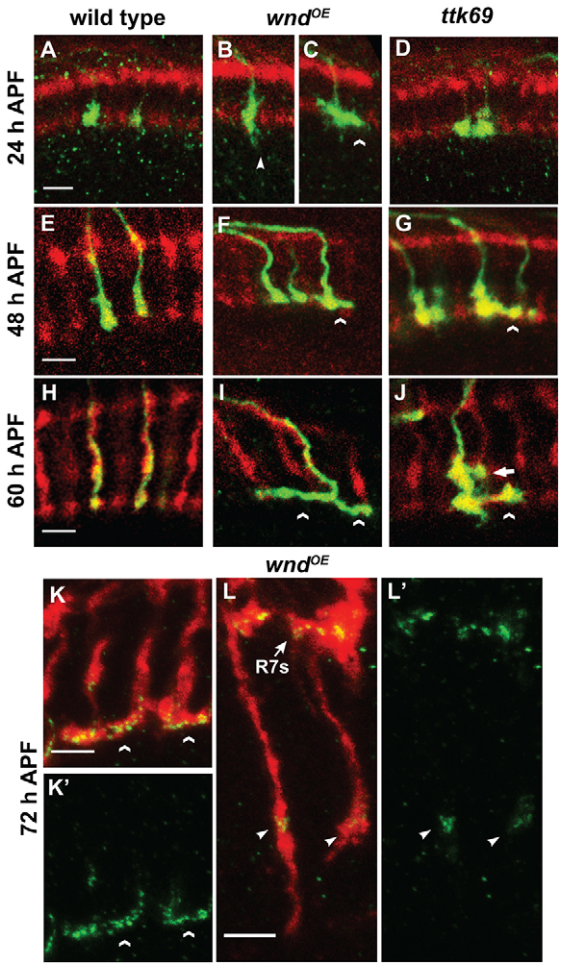

Fig. 4. Wnd overexpression and Ttk69 loss cause similar defects in R7 bouton development. (A-J) Pupal medullas (25°C) in which homozygous R7 clones generated by *GMR-FLP*/MARCM express mCD8-GFP (green). All R7 and R8 axons are labeled with anti-Chp (red). (A,E,H) Wild-type (homozygous *FRT82*) R7 axon terminals are roughly spherical at all time points and, by 60 h APF, rarely contact their neighbors (0.4±0.25%; *n*=11 brains). By contrast, at 24 h APF (B), R7s overexpressing Wnd have elongated axon terminals that partly extend beyond the R7 target layer (arrowhead), although some expand into neighboring terminals (C; chevron). During their transition into non-motile boutons, the growth cones of R7s overexpressing Wnd have axon terminals that extend laterally and overlap with their wild-type neighbors (chevrons in F,I; 11.3±0.97% at 60 h APF; *n*=14). Although *ttk69* mutant R7 growth cones are indistinguishable from wild type at 24 h APF (D), they also extend laterally and overlap with their wild-type neighbors in both the M6 (chevrons) and M3 (arrow in J) layers when they should instead be becoming stationary boutons (G,J; 23.8±1.9% at 60 h APF; *n*=7). (K-L′) Pupal medullas (25°C) in which R7s overexpress Wnd and also express endogenous levels of the active zone marker Brp-GFP (green) by means of the STaR technique (Chen et al., 2014). (K,K′) Brp-GFP puncta accumulate within the M6 layer, as in wild type, but are also present in R7 axons that extend laterally within M6 (chevrons). Brp-GFP puncta localize similarly in R7s expressing *ttk* RNAi (data not shown). (L,L′) By contrast, Brp-GFP puncta are absent from most processes that Wnd-overexpressing R7s extend beyond the M6 layer (50 of 76 processes scored lacked GFP; arrow points to the M6 layer); when present, the puncta accumulate adjacent to medulla neuropil (arrowheads; see supplementary Materials and Methods for more details on Brp-GFP localization). Scale bars: 5 µm.

As R7 growth cones become boutons, Wnd overexpression disrupts the reorientation of microtubule-containing processes and the downregulation of their extension and retraction rates

The DLK/JNK pathway is known to regulate microtubule organization and stability (Hirai et al., 2002, 2006, 2011; Lewcock et al., 2007; Eto et al., 2010; Hendricks and Jesuthasan, 2009; Feltrin et al., 2012; Ghosh-Roy et al., 2012), but its specific effect on the transition from motile growth cone to stable bouton has not been examined. Having established that increased Wnd disrupts this transition, we wanted to determine the mechanism in more detail. To do so, we caused R7s to express GFP-tagged EB1, which binds microtubule plus-ends (Rolls et al., 2007), and we imaged their axon terminals in unfixed *ex vivo* brains. We found that even in static images these preparations allowed us to detect more details of R7 axon terminal morphology than are visible in fixed samples. We focused on two time points during R7 bouton development. At 40 h APF, wild-type R7 axon terminals are still expanded (Fig. 6A,G), most have two or more EB1-GFP-containing processes of at least 0.5 µm extended at any given time (Fig. 6H), and these processes are primarily oriented at 180° relative to the axon shaft (Fig. 6I). By 48 h APF, wild-type R7 axon terminals have condensed significantly (Fig. 6D,G), most have only one EB1-containing process (Fig. 6H), and that process is even more likely to extend directly forward (Fig. 6I). In addition, both the average extension and retraction rates of EB1-containing processes decrease significantly between the two time points (Fig. 7A,B,G,H; Movies 1 and 2).

We next quantified the behavior of R7s that overexpress Wnd. At 40 h APF, their axon terminals are of normal size (Fig. 6B,G), and their EB1-containing processes have normal average extension and retraction rates (Fig. 7C,G,H; Movie 3). However, each terminal extends significantly more processes (Fig. 6H), and these processes are less likely to be oriented at 180° (Fig. 6I). By 48 h APF, Wnd-overexpressing R7 axon terminals have condensed (Fig. 6E,G) and reduced their number of processes (Fig. 6H), similar to wild type. However, these processes remain less forward-oriented (Fig. 6I) and fail to reduce their extension and retraction rates (Fig. 7D,G,H; Movie 4). These results support a model in which Wnd does not specifically promote microtubule assembly or disassembly in R7s but instead increases overall microtubule movement and disrupts microtubule orientation (Fig. 8).

Wnd overexpression and Ttk69 loss have overlapping but distinct effects on R7 bouton development

The defects in R7 bouton development caused by Ttk69 loss are similar to those caused by Wnd gain but are more frequent and severe (Kniss et al., 2013). We wanted to determine whether this is

Development (2016) 143, 2983-2993 doi:10.1242/dev.134403

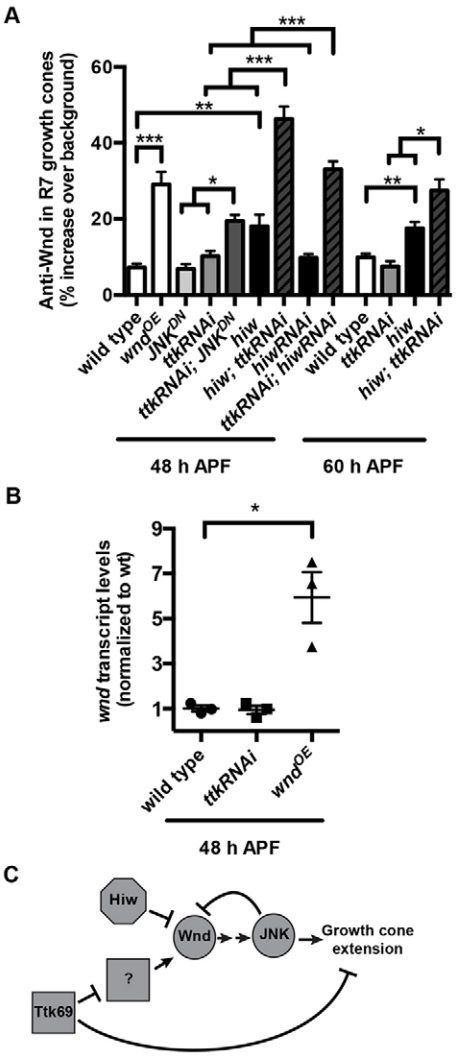

Fig. 5. As R7 growth cones become presynaptic boutons, Ttk69 acts in parallel with Hiw and JNK-dependent negative feedback to repress Wnd. (A) Quantification of anti-Wnd levels in R7 axon terminals at 48 and 60 h APF (29°C). Loss of *hiw* alone moderately increases Wnd levels in R7 axon terminals at both time points (note: values for wild type and *hiw* mutant at 60 h APF are reproduced from Fig. 1). This increase is significantly less than that caused by *chp-Gal4*-driven expression of *UAS-wnd* (*wnd*^{OE}). Loss of *ttk69* alone from R neurons (caused by *ttk* RNAi) has no significant effect on Wnd levels in R7 axon terminals. However, loss of both *hiw* and *ttk69* causes a striking, significantly greater-than-additive increase in Wnd levels in R7 terminals at both time points. This increase was observed not only when R neurons expressed *ttk* RNAi in *hiw* null mutant animals but also when R neurons co-expressed *ttk* RNAi and *hiw* RNAi. Similarly, loss of *JNK* alone (caused by *JNK*^{DN}) has no significant effect on Wnd levels, but loss of both *JNK* and *ttk69* (caused by co-expression of *ttk* RNAi and *JNK*^{DN}) results in a significantly greater-than-additive increase in Wnd levels in R7 axon terminals. **P*<0.01, ***P*<0.001 and ****P*<0.0001 based either on two-tailed *t*-tests for pairwise comparisons or a two-way ANOVA to test for greater-than-additive effects of disrupting two genes (Slinker, 1998). Error bars represent s.e.m. *n*=19, 12, 11, 12, 19, 15, 11, 21, 16, 16, 17, 8 and 11 brains from left to right on the graph. (B) Quantification of retinal *wnd* transcript levels at 48 h APF measured by qRT-PCR. Retinas in which all R neurons express *ttk* RNAi under the control of *chp-Gal4* have *wnd* transcript levels that are not significantly different from those in wild type; retinas in which R neurons express *wnd* under the control of *chp-Gal4* do have significantly increased *wnd* transcript levels (**P*<0.01). *n*=3 biological replicates, error bars represent s.e.m. (C) Model summarizing the roles of Hiw, Wnd, JNK and Ttk69 in R7s as their growth cones become presynaptic boutons.

because Ttk69 loss has a similar but more severe effect on R7 growth cone dynamics or if instead Ttk69 loss causes a distinct defect. Our results suggest that the latter is the case. Like Wnd overexpression, Ttk69 loss disrupts the forward reorientation of EB1-GFP-containing processes as R7 growth cones become boutons (Fig. 6I) and prevents the normal reduction of process extension rate (Fig. 7F,G; Movie 5). However, unlike Wnd overexpression, Ttk69 loss also prevents R7 axon terminals from condensing (Fig. 6F,G) and decreasing the number of their EB1 processes (Fig. 6H), and does not prevent them from reducing their process retraction rate (Fig. 7F,H; Movie 6). Perhaps as a consequence of disrupting the balance between retraction and extension, the length of EB1-containing processes increases significantly (Fig. 7I).

We previously found that Ttk69 promotes R7 bouton development, in part, by promoting Activin/Baboon (Babo) signaling (Kniss et al., 2013). We therefore examined whether the difference between Wnd gain and Ttk69 loss might be explained by the latter's effect on Activin/Babo. Consistent with this possibility, we found that Babo loss, like Ttk69 loss, specifically increases the average process extension rate of R7s (Fig. 7G,H). However, we also found that Babo loss, unlike Ttk69 loss, does not increase average R7 process length (Fig. 7I) or number (Fig. 6H), confirming that Ttk69 does not act exclusively through this pathway. We conclude that Ttk69 is likely to coordinate the regulation of multiple factors that influence the behavior of R7 growth cones as they become boutons.

DISCUSSION

Wnd levels in developing R7s are temporally regulated by Ttk69

Elevated DLK protein levels enhance a neuron's ability to repair axon damage but impair its ability to form appropriate connections during development. DLK levels must therefore be carefully regulated. Here, we show that, like other neurons, R7s use a PHR protein, Hiw, to keep Wnd levels low enough for their growth cones to halt properly at their targets. However, R7s later deploy a transcription factor, Ttk69, in parallel with Hiw to repress Wnd as their growth cones develop into presynaptic boutons. This temporal repression of DLK has not previously been reported but would make sense if growth cones become less tolerant of stochastic fluctuations in DLK as they are becoming boutons. However, by adding PHR-independent mechanisms of DLK repression, maturing neurons would presumably express less DLK upon injury: in R7s, for example, Ttk69 would presumably continue to repress Wnd even if injury were to release Wnd from Hiw-mediated repression. In worm, the diminished capacity of older adults to recover from axon injury is caused by such a mechanism: as adult worms age, insulin/IGF1 signaling represses DLK transcription, thereby limiting the increase in DLK after injury (Byrne et al., 2014). Our findings suggest that temporal control of DLK during development is used to protect connectivity despite potentially limiting regenerative capacity.

Wnd levels in R7s are repressed by JNK-mediated negative feedback

Like most signal transduction cascades, MAPK pathways can contain negative or positive feedback (Brummer et al., 2003; Fritsche-Guenther et al., 2011). In mouse neurons undergoing injury, JNK provides positive feedback within the DLK pathway by directly phosphorylating and thereby stabilizing DLK (Huntwork-Rodriguez et al., 2013). By contrast, in R7s, JNK provides negative feedback within the DLK pathway by decreasing DLK protein

Development (2016) 143, 2983-2993 doi:10.1242/dev.134403

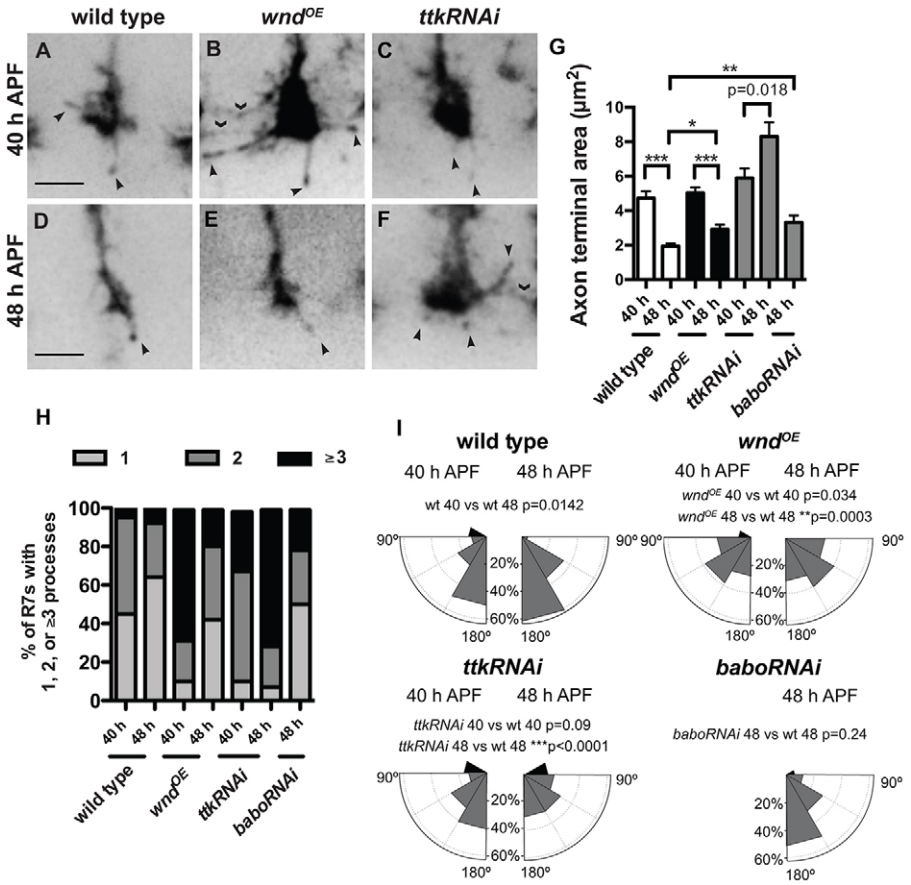

Fig. 6. Wnd overexpression and Ttk69 loss have overlapping but distinct effects on the morphology of R7 growth cones as they become boutons. (A-F) Live R7 axon terminals labeled with *chp-Gal4, UAS-EB1-GFP* at 40 and 48 h APF (29°C) extend thin, EB1-GFP-positive processes (arrowheads). Driving *wnd* or *ttk* RNAi expression in R7s causes these processes to contact neighboring terminals (chevrons). Scale bars: 3 µm. (G,H) Quantifications of EB1-GFP-positive processes. Error bars represent s.e.m. *n*=20, 27, 30, 23, 22, 16 and 18 terminals from left to right on the graphs. The areas of both wild-type (A,D) and *wnd*-overexpressing R7 axon terminals (B,E) decrease significantly as they become boutons (compare 40 and 48 h APF; G). By contrast, loss of *ttk69* causes R7 axon terminals to increase in area (C,F,G). *babo* RNAi-expressing R7 axon terminals are abnormally large at 48 h APF but not as large as those expressing *ttk* RNAi (G). **P*<0.01, ***P*<0.001, and ****P*<0.0001 based on two-tailed *t*-tests. (H) *wnd* overexpression increases the number of EB1-GFP-positive R7 processes present at 40 h APF (*P*<0.0001 based on Fisher's exact test), but the number of these processes decreases to wild-type levels by 48 h APF. By contrast, *ttk* RNAi causes an increase in process number that increases further by 48 h APF (*P*<0.0001 compared with wild type, Fisher's exact test). R7s expressing *babo* RNAi have a wild-type number of processes at 48 h APF. Only processes ≥0.5 µm in length were counted. (I) Histogram plots of R7 process angles relative to the axon shaft. Most wild-type EB1-GFP-positive processes point 'forward' (at angles between 150° and 180°) even at 40 h APF (*n*=30 processes), and the proportion that do so increases by 48 h APF (*n*=36). By contrast, R7s overexpressing *wnd* have a broader distribution of process angles at both time points, and the proportion that point forward does not increase between 40 (*n*=60) and 48 h APF (*n*=33). *ttk69* RNAi does not disrupt the primarily forward orientation of R7 processes at 40 h APF (*n*=45), but does so by 48 h APF (*n*=42). Finally, *babo* RNAi does not disrupt R7 process orientation even at 48 h APF (*n*=22). *P* values are based on Kolmogorov–Smirnov tests.

levels. One possibility is that positive and negative feedback co-exist in the DLK pathway in mouse and fly. Negative feedback occurs during development, when the pathway must be restrained, whereas positive feedback takes over upon injury, in order to promote a swift and sustained DLK response. Alternatively, our result may reflect a cell- or species-specific mechanism. In support of the latter possibility, the sites within mouse DLK that are known to be phosphorylated by JNK are not conserved in fly Wnd (Huntwork-Rodrigues et al., 2013). However, one conserved but untested MAPK consensus phosphorylation site, S643 in mouse and S715 in fly, remains a candidate for phosphorylation and consequent regulation by JNK in both species.

The R7 growth cone defect caused by Wnd overexpression changes over time

Wnd overexpression in R7s causes two distinct defects: their growth cones initially extend thin processes beyond their targets; these processes are later eliminated and instead the growth cones extend laterally. Each defect resembles one or more observed in other systems (for example, Lewcock et al. (2007) and Wang et al. (2013), respectively). However, why the defect changes over time is unclear. At each time point, the R7 growth cones maintain contact with the correct target layer, consistent with previous evidence that DLK overexpression does not prevent growth cones from responding to extrinsic cues (Lewcock et al., 2007; Shin and DiAntonio, 2011). One possibility is that the extrinsic medullar environment initially allows Wnd-overexpressing R7 growth cones to send out forward-oriented processes but later constrains them, causing them to 'burst out' laterally. Our finding that Brp puncta are present within the abnormal lateral extensions in M6 but absent from forward-oriented processes suggests a model in which the lateral extensions are preferentially stabilized by the same adhesive interactions with M6 that cause active zones to be assembled within them. Alternatively, an intrinsic R7 developmental program might

Development (2016) 143, 2983-2993 doi:10.1242/dev.134403

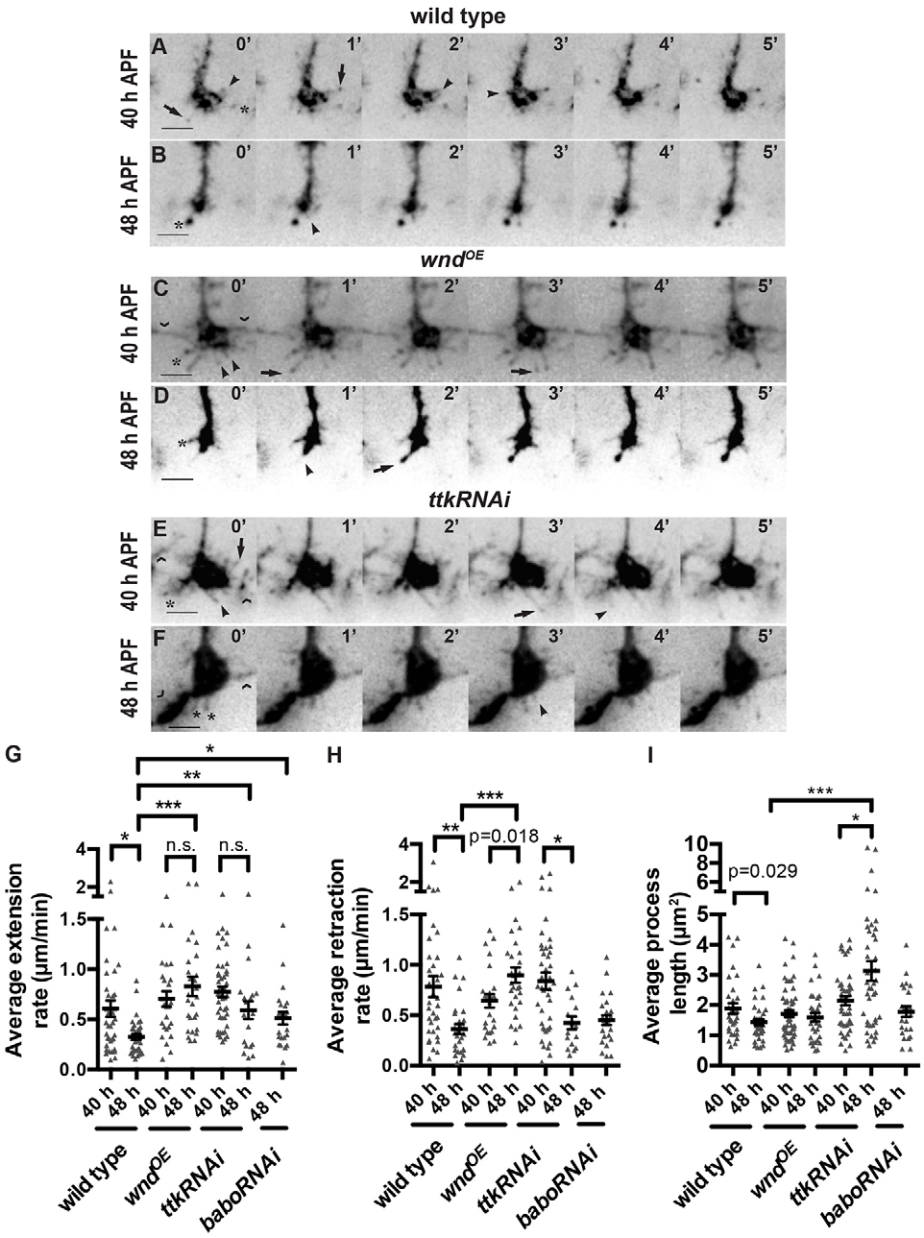

Fig. 7. Wnd overexpression and Ttk69 loss have overlapping but distinct effects on the dynamics of R7 growth cones as they become boutons. (A-F) Images of live R7 axon terminals labeled with *chp-Gal4, UAS-EB1-GFP* at 40 and 48 h APF (29°C) at 1-min intervals. Scale bars: 3 µm. Arrowheads mark onsets of extensions, arrows mark onsets of retractions. In all genotypes, some processes remain stationary (asterisks). Processes that contact neighboring terminals (chevrons) were excluded from our analysis. (G-I) Quantifications of EB1-GFP-positive processes. Error bars represent s.e.m. *P<0.01, **P<0.001, ***P<0.0001 based on pairwise two-tailed t-tests. From left to right on the graphs: n=37, 35, 26, 27, 44, 20 and 23 processes (G); n=34, 29, 24, 29, 42, 16 and 25 processes (H); n=30, 36, 60, 33, 45, 42 and 22 processes (I). The rates at which wild-type EB1-GFP-containing processes extend and retract decrease significantly as R7 terminals become boutons (compare 40 and 48 h APF; A,B,G,H). Wnd overexpression (C,D) prevents these decreases (G,H). Ttk69 loss (E,F) and Babo loss only prevent the decrease in extension rate (G,H). Ttk69 loss increases average process length (I).

be responsible. DLK can switch between promoting microtubule stability and instability at different stages of a neuron's development (Hirai et al., 2011). Perhaps increased Wnd propels R7 axon shafts forward when R7 growth cones are already moving forward but has a different effect as R7 terminals are attempting to become stationary boutons.

To examine this in more detail, we used live imaging of EB1-GFP to follow the effect of Wnd on R7 microtubules. The high levels of EB1-GFP required to visualize R7s prevented us from observing 'comets' (Morrison et al., 2002), but a comparison of our observations with a recent R7 study using a membrane-bound GFP (Özel et al., 2015) suggests that even overexpressed EB1-GFP remains associated with microtubules: we counted fewer GFP-positive processes than were observed with the membrane-bound GFP, and our processes extended and retracted at lower rates. We therefore believe our analysis reflects the behavior of pioneer microtubules, which escape the growth cone's central domain and explore a subset of actin-based growth cone filopodia (Lowery and Van Vactor, 2009; Bearce et al., 2015). We found that Wnd overexpression increases the number of EB1 processes in younger R7s (40 h APF), suggesting that Wnd initially promotes microtubule stability. However, Wnd does not prevent older R7 growth cones from condensing or decreasing their number of EB1 processes and instead increases the overall movement of EB1 processes, suggesting that Wnd does not promote microtubule stability during bouton development. The additional disruption of microtubule orientation by Wnd could account for the lateral extensions, as the orientation of pioneer microtubules is strongly associated with the direction of growth cone consolidation (Bearce et al., 2015).

Ttk69 coordinates multiple pathways that regulate growth cone behavior

We performed several experiments to test the functional significance of the increased Wnd expression in R7s when both Hiw and Ttk69 are disrupted. We found that loss of *hiw* did not

Development (2016) 143, 2983-2993 doi:10.1242/dev.134403

A

	wild type	wnd^{OE}	ttkRNAi
Growth cone area	↓	↓	↑
Process number	↓	↓	↑
Process length	↓	No change	↑
Rate of process extension	↓	No change	No change
Rate of process retraction	↓	No change	↓
Proportion of non-forward oriented processes	↓	No change	No change

B

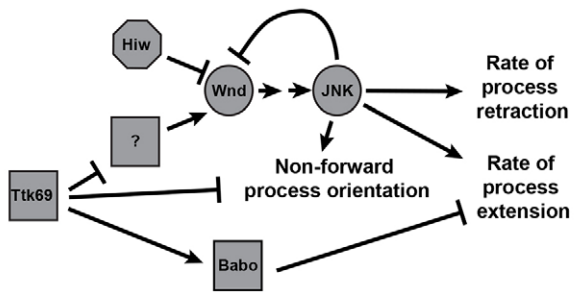

Fig. 8. Model of how Wnd and Ttk69 affect the development of R7 growth cones into presynaptic boutons. (A) Table summarizing results from Figs 6 and 7. In wild type, all properties listed decrease (black arrows) as growth cones become boutons. Wnd overexpression or Ttk69 loss causes some properties to increase (red arrows) whereas others remain unchanged. (B) Model consistent with the pathway relationships summarized in Fig. 5C and the phenotypes summarized in A, as well as with previous data on the pathway relationship between Ttk69 and Babo (Kniss et al., 2013) and the new data on Babo loss from Figs 6 and 7.

enhance the R7 defect caused by Ttk69 loss (Fig. S3C-I). Nor did disrupting Wnd or JNK ameliorate the R7 defect caused by Ttk69 loss (Fig. S3C-I). We also found that loss of Ttk69 and overexpression of Wnd have overlapping but distinct effects on the morphology and behavior of R7 growth cones. Together, these results are consistent with Ttk69 acting upstream of one or more additional regulators of growth cone dynamics that act in parallel with the Wnd/JNK pathway: in the absence of Ttk69, these other regulators severely disrupt R7 growth cone behavior whether or not Wnd is further increased or decreased (Fig. 8B).

MATERIALS AND METHODS

Flies

Drosophila melanogaster were raised at 25°C (Fig. 2A-F; Fig. 3A-F′; Fig. 4) or 29°C (Fig. 1; Fig. 2G; Fig. 3G,H; Figs 5-7). We observed no difference between the sexes. For strains and genotypes, see supplementary Materials and Methods.

Fixed images

Brains were dissected, fixed and stained as in Miller et al. (2008). Staining was done in parallel with controls, and phenotypes were scored blind. Images were collected on a Leica SP2 microscope and analyzed using Fiji (http://fiji.sc; Schindelin et al., 2012). For a list of antibodies, see supplementary Materials and Methods. Brp puncta within R7 terminals were labeled by the STaR method as in Chen et al. (2014), using *20C11-FLP* and *chp-Gal4*. To quantify Wnd protein levels in R7 axon terminals, we generated regions of interest (ROIs) by tracing ∼20 R7 terminals per optic lobe while blind to the anti-Wnd channel (Fig. S1A-B′). We then measured anti-Wnd fluorescence intensities within these ROIs. To control for variability in immunostaining, we normalized the average anti-Wnd intensity in R7s of each brain to the average anti-Wnd fluorescence intensity of adjacent medulla neuropil (Fig. S1A-C). See supplementary Materials and Methods for additional details on our quantification of R7 phenotypes. All images, ROIs and raw data are available upon request.

Live images

We adapted the protocol of Williamson and Hiesinger (2010): each pupa was removed from its case and its head isolated in HL3 (Broadie, 2000) with visual system intact. Brains taken at 40 h APF required no further dissection. Brains taken at 48 h APF often required further removal of cuticle from the posterior head for optical access. Brains and fat bodies were transferred together in HL3 to imaging chambers (Cabernard and Doe, 2013) and immobilized using WormGlu (Glushield) on gas-permeable membranes (YSI). Brains were mounted dorsal-side down and images acquired from the ventral, posterior part of the medulla at a depth of three to four R7 axon terminals. We used a Leica DMI400B spinning disk microscope to image ∼3 µm *z*-stacks (acquired in 0.3 µm *z*-steps) at 30 s intervals during a 30 min period. Images were processed using Fiji: we generated max projections of seven to ten *z*-steps encompassing the total thickness of an R7 terminal and corrected for lateral drift using TurboReg. The length of each process was measured from the edge of the pixel-dense growth cone to the tip of each projection. Discrete extension and retraction events (defined as a change in length of at least 0.5 µm) were identified manually, and the lengths of processes at the beginning and the end of each event (defined as a pause or a reversal in direction) were measured to determine average rates (calculated by dividing the change in length by the change in time during a given event). Instantaneous velocity was not measured. All images and raw data are available upon request.

Quantitative RT-PCR

qRT-PCR was performed using KAPA SYBR FAST ABI Prism qPCR master mix (Kapa Biosystems) on cDNA synthesized using oligo $(dT)_{18}$ primer and Maxima H-Minus reverse transcriptase (Thermo Scientific). cDNAs were generated from 1 µg of Trizol-isolated RNA from 10-20 pairs of dissected pupal retinas per biological replicate. Retinas were dissected on ice and tissue flash-frozen in Trizol. Relative mRNA expression was normalized using a control transcript (*RpL32*) to calculate ΔCTs (threshold cycles). Expression level comparisons between genetic manipulations or developmental time points were made using the ΔΔCT method. ΔCT values were used for two-tailed *t*-tests to determine statistical significance. See supplementary Materials and Methods for primer sequences. Raw CT values are available upon request.

Acknowledgements

We thank C. Collins and the Developmental Studies Hybridoma Bank for antibodies, and C. Collins, C. Doe, S. L. Zipursky, the Bloomington *Drosophila* Stock Center, and the Vienna *Drosophila* Resource Center for fly stocks. We thank J. Eisen for comments on the manuscript.

Competing interests

The authors declare no competing or financial interests.

Author contributions

A.I.F. and T.G.H. designed experiments; A.I.F. performed all experiments; A.I.F. and T.G.H. wrote the manuscript.

Funding

This work was supported by a National Institutes of Health (NIH) National Research Service Award training grant [5-T32-GM007413-35 to A.I.F.] and an NIH grant [R01 EY019694 to T.G.H.]. Deposited in PMC for release after 12 months.

Supplementary information

Supplementary information available online at
http://dev.biologists.org/lookup/doi/10.1242/dev.134403.supplemental

Development (2016) 143, 2983-2993 doi:10.1242/dev.134403

References

Baker, S. T., Opperman, K. J., Tulgren, E. D., Turgeon, S. M., Bienvenut, W. and Grill, B. (2014). RPM-1 uses both ubiquitin ligase and phosphatase-based mechanisms to regulate DLK-1 during neuronal development. *PLOS Genet.* **10**, e1004297.

Bearce, E. A., Erdogan, B. and Lowery, L. A. (2015). TIPsy tour guides: how microtubule plus-end tracking proteins (+TIPs) facilitate axon guidance. *Front. Cell. Neurosci.* **9**, 241.

Bloom, A. J., Miller, B. R., Sanes, J. R. and DiAntonio, A. (2007). The requirement for Phr1 in CNS axon tract formation reveals the corticostriatal boundary as a choice point for cortical axons. *Genes Dev.* **21**, 2593-2606.

Bossuyt, W., De Geest, N., Aerts, S., Leenaerts, I., Marynen, P. and Hassan, B. A. (2009). The atonal proneural transcription factor links differentiation and tumor formation in Drosophila. *PLoS Biol.* **7**, e1000040.

Brace, E. J., Wu, C., Valakh, V. and DiAntonio, A. (2014). SkpA restrains synaptic terminal growth during development and promotes axonal degeneration following injury. *J. Neurosci.* **34**, 8398-8410.

Broadie, K. (2000). Electrophysiological approaches to the neuromusculature. In *Drosophila Protocols* (ed. W. Sullivan, M. Ashburner and R. S. Hawley), pp. 274-275. Cold Spring Harbor, NY: CSHLP.

Brummer, T., Naegele, H., Reth, M. and Misawa, Y. (2003). Identification of novel ERK-mediated feedback phosphorylation sites at the C-terminus of B-Raf. *Oncogene* **22**, 8823-8834.

Burgess, R. W., Peterson, K. A., Johnson, M. J., Roix, J. J., Welsh, I. C. and O'Brien, T. P. (2004). Evidence for a conserved function in synapse formation reveals Phr1 as a candidate gene for respiratory failure in newborn mice. *Mol. Cell. Biol.* **24**, 1096-1105.

Byrne, A. B., Walradt, T., Gardner, K. E., Hubbert, A., Reinke, V. and Hammarlund, M. (2014). Insulin/IGF1 signaling inhibits age-dependent axon regeneration. *Neuron* **81**, 561-573.

Cabernard, C. and Doe, C. Q. (2013). Live imaging of neuroblast lineages within intact larval brains in *Drosophila*. *Cold Spring Harb. Protoc.* **2013**, 970-977.

Chen, Y., Akin, O., Nern, A., Tsui, C. Y. K., Pecot, M. Y. and Zipursky, S. L. (2014). Cell-type-specific labeling of synapses in vivo through synaptic tagging with recombination. *Neuron* **81**, 280-293.

Collins, C. A., Wairkar, Y. P., Johnson, S. L. and DiAntonio, A. (2006). Highwire restrains synaptic growth by attenuating a MAP kinase signal. *Neuron* **51**, 57-69.

Dietz, G., Chen, D., Schnorrer, F., Su, K.-C., Barinova, Y., Fellner, M., Gasser, B., Kinsey, K., Oppel, S., Scheiblauer, S. et al. (2007). A genome-wide transgenic RNAi library for conditional gene inactivation in *Drosophila*. *Nature* **448**, 151-156.

D'Souza, J., Hendricks, M., Le Guyader, S., Subburaju, S., Grunewald, B., Scholich, K. and Jesuthasan, S. (2005). Formation of the retinotectal projection requires Esrom, an ortholog of PAM (protein associated with Myc). *Development* **132**, 247-256.

Eto, K., Kawauchi, T., Osawa, M., Tabata, H. and Nakajima, K. (2010). Role of dual leucine zipper-bearing kinase (DLK/MUK/ZPK) in axonal growth. *Neurosci. Res.* **66**, 37-45.

Feltrin, D., Fusco, L., Witte, H., Moretti, F., Martin, K., Letzelter, M., Fluri, E., Scheiffele, P. and Pertz, O. (2012). Growth cone MKK7 mRNA targeting regulates MAP1b-dependent microtubule bundling to control neurite elongation. *PLoS Biol.* **10**, e1001439.

Fernandes, K. A., Harder, J. M., John, S. W., Shrager, P. and Libby, R. T. (2014). DLK-dependent signaling is important for somal but not axonal degeneration of retinal ganglion cells following axonal injury. *Neurobiol. Dis.* **69**, 108-116.

Fritsche-Guenther, R., Witzel, F., Sieber, A., Herr, R., Schmidt, N., Braun, S., Brummer, T., Sers, C. and Blüthgen, N. (2011). Strong negative feedback from Erk to Raf confers robustness to MAPK signalling. *Mol. Syst. Biol.* **7**, 489.

Ghosh-Roy, A., Goncharov, A., Jin, Y. and Chisholm, A. D. (2012). Kinesin-13 and tubulin posttranslational modifications regulate microtubule growth in axon regeneration. *Dev. Cell* **23**, 716-728.

Godement, P., Wang, L. C. and Mason, C. A. (1994). Retinal axon divergence in the optic chiasm: dynamics of growth cone behavior at the midline. *J. Neurosci.* **14**, 7024-7039.

Goldberg, J. L. (2004). Intrinsic neuronal regulation of axon and dendrite growth. *Curr. Opin. Neurobiol.* **14**, 551-557.

Grill, B., Bienvenut, W. V., Brown, H. M., Ackley, B. D., Quadroni, M. and Jin, Y. (2007). C. elegans RPM-1 regulates axon termination and synaptogenesis through the Rab GEF GLO-4 and the Rab GTPase GLO-1. *Neuron* **55**, 587-601.

Hammarlund, M., Nix, P., Hauth, L., Jorgensen, E. M. and Bastiani, M. (2009). Axon regeneration requires a conserved MAP kinase pathway. *Science* **323**, 802-806.

Hendricks, M. and Jesuthasan, S. (2009). PHR regulates growth cone pausing at intermediate targets through microtubule disassembly. *J. Neurosci.* **29**, 6593-6598.

Hendricks, M., Mathuru, A. S., Wang, H., Silander, O., Kee, M. Z. L. and Jesuthasan, S. (2008). Disruption of Esrom and Ryk identifies the roof plate boundary as an intermediate target for commissure formation. *Mol. Cell. Neurosci.* **37**, 271-283.

Hirai, S.-I., Kawaguchi, A., Hirasawa, R., Baba, M., Ohnishi, T. and Ohno, S. (2002). MAPK-upstream protein kinase (MUK) regulates the radial migration of immature neurons in telencephalon of mouse embryo. *Development* **129**, 4483-4495.

Hirai, S.-i., Cui, D. F., Miyata, T., Ogawa, M., Kiyonari, H., Suda, Y., Aizawa, S., Banba, Y. and Ohno, S. (2006). The c-Jun N-terminal kinase activator dual leucine zipper kinase regulates axon growth and neuronal migration in the developing cerebral cortex. *J. Neurosci.* **26**, 11992-12002.

Hirai, S.-i., Banba, Y., Satake, T. and Ohno, S. (2011). Axon formation in neocortical neurons depends on stage-specific regulation of microtubule stability by the dual leucine zipper kinase-c-Jun N-terminal kinase pathway. *J. Neurosci.* **31**, 6468-6480.

Huntwork-Rodriguez, S., Wang, B., Watkins, T. A., Ghosh, A. S., Pozniak, C. D., Bustos, D., Newton, K., Kirkpatrick, D. S. and Lewcock, J. W. (2013). JNK-mediated phosphorylation of DLK suppresses its ubiquitination to promote neuronal apoptosis. *J. Cell Biol.* **202**, 747-763.

Klinedinst, S., Wang, X., Xiong, X., Haenfler, J. M. and Collins, C. A. (2013). Independent pathways downstream of the Wnd/DLK MAPKKK regulate synaptic structure, axonal transport, and injury signaling. *J. Neurosci.* **33**, 12764-12778.

Kniss, J. S., Holbrook, S. and Herman, T. G. (2013). R7 photoreceptor axon growth is temporally controlled by the transcription factor Ttk69, which inhibits growth in part by promoting transforming growth factor-β/activin signaling. *J. Neurosci.* **33**, 1509-1520.

Langen, M., Agi, E., Altschuler, D. J., Wu, F., Altschuler, S. J. and Hiesinger, P. R. (2015). The developmental rules of neural superposition in *Drosophila*. *Cell* **162**, 120-133.

Lee, T. and Luo, L. (1999). Mosaic analysis with a repressible cell marker for studies of gene function in neuronal morphogenesis. *Neuron* **22**, 451-461.

Lee, C.-H., Herman, T. G., Clandinin, T. R., Lee, R. and Zipursky, S. L. (2001). N-cadherin regulates target specificity in the *Drosophila* visual system. *Neuron* **30**, 437-450.

Lewcock, J. W., Genoud, N., Lettieri, K. and Pfaff, S. L. (2007). The ubiquitin ligase Phr1 regulates axon outgrowth through modulation of microtubule dynamics. *Neuron* **56**, 604-620.

Li, H., Kulkarni, G. and Wadsworth, W. G. (2008). RPM-1, a *Caenorhabditis elegans* protein that functions in presynaptic differentiation, negatively regulates axon outgrowth by controlling SAX-3/robo and UNC-5/UNC5 activity. *J. Neurosci.* **28**, 3595-3603.

Liao, E. H., Hung, W., Abrams, B. and Zhen, M. (2004). An SCF-like ubiquitin ligase complex that controls presynaptic differentiation. *Nature* **430**, 345-350.

Lowery, L. A. and Van Vactor, D. (2009). The trip of the tip: understanding the growth cone machinery. *Nat. Rev. Mol. Cell Biol.* **10**, 332-343.

Mar, F. M., Bonni, A. and Sousa, M. M. (2014). Cell intrinsic control of axon regeneration. *EMBO Rep.* **15**, 254-263.

McCabe, B. D., Hom, S., Aberle, H., Fetter, R. D., Marques, G., Haerry, T. E., Wan, H., O'Connor, M. B., Goodman, C. S. and Haghighi, A. P. (2004). Highwire regulates presynaptic BMP signaling essential for synaptic growth. *Neuron* **41**, 891-905.

Meinertzhagen, I. A. and Hanson, T. E. (1993). The development of the optic lobe. In *The Development of Drosophila melanogaster*, Vol II (ed. M. Bate and A. Martinez Arias), pp. 1363-1491. Cold Spring Harbor, NY: CSHLP.

Miller, A. C., Seymour, H., King, C. and Herman, T. G. (2008). Loss of *seven-up* from *Drosophila* R1/R6 photoreceptors reveals a stochastic fate choice that is normally biased by Notch. *Development* **135**, 707-715.

Moore, D. L. and Goldberg, J. L. (2011). Multiple transcription factor families regulate axon growth and regeneration. *Dev. Neurobiol.* **71**, 1186-1211.

Morrison, E. E., Moncur, P. M. and Askham, J. M. (2002). EB1 identifies sites of microtubule polymerisation during neurite development. *Mol. Brain Res.* **98**, 145-152.

Nakata, K., Abrams, B., Grill, B., Goncharov, A., Huang, X., Chisholm, A. D. and Jin, Y. (2005). Regulation of a DLK-1 and p38 MAP kinase pathway by the ubiquitin ligase RPM-1 is required for presynaptic development. *Cell* **120**, 407-420.

Ni, J.-Q., Liu, L.-P., Binari, R., Hardy, R., Shim, H.-S., Cavallaro, A., Booker, M., Pfeiffer, B. D., Markstein, M., Wang, H. et al. (2009). A *Drosophila* resource of transgenic RNAi lines for neurogenetics. *Genetics* **182**, 1089-1100.

Nix, P., Hisamoto, N., Matsumoto, K. and Bastiani, M. (2011). Axon regeneration requires coordinate activation of p38 and JNK MAPK pathways. *Proc. Natl. Acad. Sci. USA* **108**, 10738-10743.

Opperman, K. J. and Grill, B. (2014). RPM-1 is localized to distinct subcellular compartments and regulates axon length in GABAergic motor neurons. *Neural Dev.* **9**, 10.

Özel, M. N., Langen, M., Hassan, B. A. and Hiesinger, P. R. (2015). Filopodial dynamics and growth cone stabilization in *Drosophila* visual circuit development. *eLife* **4**, e10721.

Rolls, M. M., Satoh, D., Clyne, P. J., Henner, A. L., Uemura, T. and Doe, C. Q. (2007). Polarity and intracellular compartmentalization of *Drosophila* neurons. *Neural Dev.* **2**, 7.

Schaefer, A. M., Gayla, H. D. and Nonet, M. L. (2000). rpm-1, a conserved neuronal gene that regulates targeting and synaptogenesis in C. elegans. *Neuron* **26**, 345-356.

Development (2016) 143, 2983-2993 doi:10.1242/dev.134403

Schindelin, J., Arganda-Carreras, I., Frise, E., Kaynig, V., Longair, M., Pietzsch, T., Preibisch, S., Rueden, C., Saalfield, S., Schmid, B. et al. (2012). Fiji: an open-source platform for biological-image analysis. *Nat. Methods* **9**, 676-682.

Sharma, J., Baker, S. T., Turgeon, S. M., Gurney, A. M., Opperman, K. J. and Grill, B. (2014). Identification of a peptide inhibitor of the RPM-1·FSN-1 ubiquitin ligase complex. *J. Biol. Chem.* **289**, 34654-34666.

Shin, J. E. and DiAntonio, A. (2011). Highwire regulates guidance of sister axons in the *Drosophila* mushroom body. *J. Neurosci.* **31**, 17689-17700.

Shin, J. E., Cho, Y., Beirowski, B., Milbrandt, J., Cavalli, V. and DiAntonio, A. (2012). Dual leucine zipper kinase is required for retrograde injury signaling and axonal regeneration. *Neuron* **74**, 1015-1022.

Slinker, B. K. (1998). The statistics of synergism. *J. Mol. Cell. Cardiol.* **30**, 723-731.

Steketee, M. B., Oboudiyat, C., Daneman, R., Trakhtenberg, E., Lamoureux, P., Weinstein, J. E., Heidemann, S., Barres, B. A. and Goldberg, J. L. (2014). Regulation of intrinsic axon growth ability at retinal ganglion cell growth cones. *Invest. Ophthalmol. Vis. Sci.* **55**, 4369-4377.

Tedeschi, A. and Bradke, F. (2013). The DLK signalling pathway—a double-edged sword in neural development and regeneration. *EMBO Rep.* **14**, 605-614.

Ting, C.-Y., Yonekura, S., Chung, P., Hsu, S.-N., Robertson, H. M., Chiba, A. and Lee, C.-H. (2005). Drosophila N-cadherin functions in the first stage of the two-stage layer-selection process of R7 photoreceptor afferents. *Development* **132**, 953-963.

Vitriol, E. A. and Zheng, J. Q. (2012). Growth cone travel in space and time: the cellular ensemble of cytoskeleton, adhesion, and membrane. *Neuron* **73**, 1068-1081.

Wang, X., Kim, J. H., Bazzi, M., Robinson, S., Collins, C. A. and Bing, Y. (2013). Bimodal control of dendritic and axonal growth by the Dual Leucine Zipper Kinase Pathway. *PLoS Biol.* **11**, e1001572.

Weber, U., Paricio, N. and Mlodzik, M. (2000). Jun mediates Frizzled-induced R3/R4 cell fate distinction and planar polarity determination in the *Drosophila* eye. *Development* **127**, 3619-3629.

Williamson, W. R. and Hiesinger, P. R. (2010). Preparation of developing and adult *Drosophila* brains and retinae for live imaging. *JoVE* **37**, 1936.

Wu, C., Wairkar, Y. P., Collins, C. A. and DiAntonio, A. (2005). Highwire function at the *Drosophila* neuromuscular junction: spatial, structural, and temporal requirements. *J. Neurosci.* **25**, 9557-9566.

Wu, C., Daniels, R. W. and DiAntonio, A. (2007). DFsn collaborates with Highwire to down-regulate the Wallenda/DLK kinase and restrain synaptic terminal growth. *Neural Dev.* **2**, 16.

Xiong, W. C. and Montell, C. (1993). Tramtrack is a transcriptional repressor required for cell fate determination in the *Drosophila* eye. *Genes Dev.* **7**, 1085-1096.

Xiong, X., Wang, X., Ewanek, R., Bhat, P., DiAntonio, A. and Collins, C. A. (2010). Protein turnover of the Wallenda/DLK kinase regulates a retrograde response to axonal injury. *J. Cell Biol.* **191**, 211-223.

Yan, D. and Jin, Y. (2012). Regulation of DLK-1 kinase activity by calcium-mediated dissociation from an inhibitory isoform. *Neuron* **76**, 534-548.

Yan, D., Wu, Z., Chisholm, A. D. and Jin, Y. (2009). The DLK-1 kinase promotes mRNA stability and local translation in C. elegans synapses and axon regeneration. *Cell* **138**, 1005-1018.

Supplementary Materials and Methods

Genetics. Flies expressing the following transgenes were used in this study: *chaoptin* (*chp*)-*Gal4* (a generous gift from S. L. Zipursky, University of California, Los Angeles, CA), *actin* (*act*)-*Gal4* (Bloomington *Drosophila* Stock Center), *PM181-Gal4* (Lee et al., 2001), *UAS-wnd* (*wnd*^{OE}; Collins et al., 2006), *UAS-Bsk*^{DN} (*JNK*^{DN}; Weber et al., 2000, Bossuyt et al., 2009), *UAS-mCD8-ChRFP* (Bloomington *Drosophila* Stock Center), *UAS-Dcr-2* (Dietz *et al* 2007), *UAS-mCD8-GFP* (Lee and Luo, 1999), *UAS-EB1-GFP* (Rolls et al., 2007), 20C11-FLP (Chen et al., 2014); brp-FSF-GFP (Chen et al., 2014), and UAS-FSF-tdTomato-myr (Chen et al., 2014). *UAS-RNAi* lines from the Vienna *Drosophila* Resource Center (Dietz et al., 2007) were used to knock down expression of Ttk69 (#101980) and Babo (#106092), and a *UAS-RNAi* stock from the Transgenic RNAi Resource Project was used to knockdown Hiw (Ni et al., 2009; Bloomington *Drosophila* Stock Center # 28031).

"wild type" animals in Fig. 1, 2G, 3, 5A, S1, S2C, S3C and S3I were *UAS-Dcr-2/+;;chp-Gal4*, *UAS-EB1-GFP/+* or *UAS-Dcr-2/Y;;chp-Gal4*, *UAS-EB1-GFP/+.*

"wild type" animals in Fig. 2A-F were *UAS-Dcr-2/+; UAS-mCD8-GFP/+; chp-Gal4/+* or *UAS-Dcr-2/Y; UAS-mCD8-GFP/+; Chp-Gal4/+.*

"wild type" animals in Fig. 5B and S3A-B were *UAS-Dcr-2/Y;;chp-Gal4*, *UAS-EB1-GFP/+.*

"wild type" animals in Fig. S2A-A'' were *+/Y;; UAS-mCD8-GFP, PM181-Gal4/+.*

"*wild type"* animals in Fig. 6, 7 were *UAS-Dcr-2;; chp-Gal4, UAS-EB1-GFP*

We used the *hiw* loss-of-function alleles *hiw*$^{\Delta N}$, *hiw*$^{\Delta C}$ and *hiw*^{ND8} (Wu et al., 2005) and found that *hiw* mutant animals of genotype *hiw*$^{\Delta N}$*/Y*, *hiw*$^{\Delta C}$*/Y*, *hiw*$^{\Delta N}$*/ hiw*$^{\Delta C}$*,* or *hiw*^{ND8}*/hiw*$^{\Delta N}$ had indistinguishable R7 phenotypes (data not shown).

'*hiw*'' mutant animals in Fig.1, 3, 5, S1 and S3 were *hiw*$^{\Delta N}$*/Y; chp-Gal4, UAS-EB1-GFP/+* or *hiw*$^{\Delta C}$*/Y; chp-Gal4, UAS-EB1-GFP/+*

"*hiw*'' mutant animals in Fig. 2 were *hiw*$^{\Delta N}$*/Y; UAS-mCD8-GFP; chp-Gal4/+*

"*hiw*'' mutant animals in Fig. S2 were *hiw*$^{\Delta N}$*/Y; UAS-mC8GFP, PM181-Gal4/+*.

"JNK^{DN}" animals in Fig. 1, 2, 3, 5A S2 and S3 were *UAS-Dcr-2/+;; chp-Gal4*, *UAS-EB1-GFP/UAS-Bsk*^{DN} or *UAS-Dcr-2/Y;;chp-Gal4*, *UAS-EB1-GFP/ UAS-Bsk*^{DN}*.*

"wnd" mutant animals in Fig. 1, 2, and S1 were *UAS-Dcr-2/w; UAS-mCD8-GFP/+; chp-Gal4, wnd*^{1}*/wnd*^{3} or *w/Y; UAS-mCD8-GFP/+; chp-Gal4, wnd*^{1}*/wnd*^{3}. This allelic combination has previously been reported to be a protein null (Wu et al., 2007).

"*hiw, wnd"* mutant animals in Fig 2D-F were *hiw*$^{\Delta N}$*; UAS-mCD8-GFP/+; chp-Gal4, wnd*^{1}*/wnd*^{3}

"*wnd*^{OE}" animals in Fig. 2G, 3, and S2 were *w; UAS-wnd/UAS-mCD8-RFP; chp-Gal4, UAS-EB1-GFP/+*or *w/Y; UAS-wnd/UAS-mCD8-RFP; chp-Gal4, UAS-EB1-GFP/+*.

"*wnd*^{OE}" animals in Fig. 4K-L' were *w; 20C11-FLP/UAS-wnd; chp-Gal4/brp-FSF-GFP, UAS-FSF-tdTomato*.

"*wnd*^{OE}" animals in Fig. 5A were *UAS-Dcr-2/w; UAS-wnd/+; chp-Gal4, UAS-EB1-GFP/+* or *UAS-Dcr-2/Y UAS-wnd/+; chp-Gal4, UAS-EB1-GFP/+*.

"*wnd*^{OE}" animals in Fig. 5B were *UAS-Dcr-2/Y UAS-wnd/+; chp-Gal4, UAS-EB1-GFP/+*.

"*wnd*^{OE}*"* animals in Fig. 6, 7 were *UAS-Dcr-2/w; UAS-wnd; chp-Gal4, UAS-EB1-GFP*

"wnd^{OE}*; JNK*^{DN}*"* animals in Fig 3G,H and S2 were *w; UAS-wnd/+; chp-Gal4, UAS-EB1-GFP/UAS-Bsk*^{DN} or *w/Y; UAS-wnd/+; chp-Gal4, UAS-EB1-GFP/UAS-Bsk*^{DN}

"hiwRNAi" animals in Fig. 5 were *UAS-Dcr-2/w; UAS-hiwRNAi/+; chp-Gal4, UAS-EB1-GFP/+* or *UAS-Dcr-2/Y; UAS-hiwRNAi/+; chp-Gal4, UAS-EB1-GFP/+*

"*ttkRNAi*" animals in Fig. 5A and S3F and S3I were *UAS-Dcr-2/Y; UAS-ttkRNAi/+; chp-Gal4, UAS-EB1-GFP/+* or *UAS-Dcr-2/+; UAS-ttkRNAi/+; chp-Gal4, UAS-EB1-GFP/+*.

"*ttkRNAI"* animals in Fig. 5A and S3F also included *w/Y; UAS-ttkRNAi/+; chp-Gal4, UAS-EB1-GFP/ UAS-Dcr-2*

"*ttkRNAi"* animals in Fig. S3I also included *UAS-Dcr-2; UAS-mCD8-GFP/UAS-ttkRNAi; chp-Gal4/+*

"*ttkRNAi*" animals in Fig. 5B, and S3B were *UAS-Dcr-2/Y; UAS-ttkRNAi/+; chp-Gal4, UAS-EB1-GFP/+.*

"*ttkRNAi"* animals in Fig. 6, 7 were *UAS-Dcr-2; UAS-ttkRNAi/+; chp-Gal4, UAS-EB1-GFP.*

"hiw, ttkRNAi" animals in Fig. 5A, S3G, I were *hiw*$^{\Delta N}$*; UAS-ttkRNAi/+; chp-Gal4, UAS-EB1-GFP/UAS-Dcr-2*

"ttkRNAi; JNK^{DN}" animals in Fig. 5 and S3 were *UAS-Dcr-2/Y; UAS-ttkRNAi/+; chp-Gal4, UAS-EB1-GFP/UAS-Bsk*^{DN} or *UAS-Dcr-2/w; UAS-ttkRNAi/+; chp-Gal4, UAS-EB1-GFP/UAS-Bsk*^{DN}.

"ttkRNAi, hiwRNAi" animals in Fig. 5 were *UAS-Dcr-2/w:; ttkRNAi/+; chp-Gal4, UAS-EB1-GFP/UAS-hiwRNAi* or *UAS-Dcr-2/Y:; ttkRNAi/+; chp-Gal4, UAS-EB1-GFP/UAS-hiwRNAi*

"*baboRNAi*" animals in Fig. 6 and 7 were *UAS-Dcr-2/Y*; *UAS-baboRNAi/+; chp-Gal4, UAS-EB1-GFP* or *UAS-Dcr-2/w*; *UAS-baboRNAi/+; chp-Gal4, UAS-EB1-GFP.*

"*ttkRNAi, wnd"* animals in Fig S3I were *UAS-Dcr-2/w; UAS-mCD8-GFP/UAS-ttkRNAi; chp-Gal4, wnd^{1}/wnd^{3}* or *UAS-Dcr-2/Y; UAS-mCD8-GFP/UAS-ttkRNAi; chp-Gal4, wnd^{1}/wnd^{3}*

In Fig. 4, homozygous wild type (*FRT82*), *ttk69* mutant (*ttk^{1e11}*; Xiong and Montell, 1993), or *UAS-wnd* overexpressing R7 clones were generated and labeled using *GMR-FLP* and MARCM (mosaic analysis with a repressible cell marker; Lee and Luo, 1999; Lee et al., 2001).

"wild type" animals in Fig. 4 were *GMR-FLP/Y*; *act-Gal4, UAS-mCD8-GFP/+; FRT82/FRT82, tub-Gal80* or *GMR-FLP/y, w*; *act-Gal4, UAS-mCD8-GFP/+; FRT82/FRT82, tub-Gal80*.

"*ttk69 mutant"* animals in Fig. 4 and S3I were *GMR-FLP/Y*; *act-Gal4, UAS-mCD8-GFP/+; FRT82, ttk^{1e11}/FRT82, tub-Gal80* or *GMR-FLP/y, w*; *act-Gal4, UAS-mCD8-GFP/+; FRT82, ttk^{1e11}/FRT82, tub-Gal80*.

"*wnd^{OE}*" animals in Fig. 4B,C,F,I were *GMR-FLP/Y*; *act-Gal4, UAS-mCD8-GFP/UAS-wnd; FRT82/FRT82, tub-Gal80* or *GMR-FLP/y, w*; *act-Gal4, UAS-mCD8-GFP/UAS-wnd; FRT82/FRT82, tub-Gal80*.

"*JNK^{DN}, ttk69"* animals in Fig. S3I were *GMR-FLP/UAS-Bsk^{DN}; act-Gal4, UAS-mCD8-GFP/+; FRT82, gal80/FRT82, ttk^{1e11}*.

Antibodies. We used the following antibodies: mouse anti-Chp (24B10; 1:200) from the Developmental Studies Hybridoma Bank; rabbit anti-Wnd (A3-1,2; 1:300; Collins et al., 2006), a generous gift from C. Collins; chicken anti-GFP (1:1000) from Abcam, rabbit anti-GFP (1:5000) and all secondary antibodies (goat IgG coupled to Alexa Fluor 488, Alexa Fluor 555, or AlexFluor 633; 1:250) from Life Technologies.

Quantification of circularity. R7 growth cone circularity was measured by acquiring shape descriptors of R7 growth cone ROIs using ImageJ software. Within each brain, 20 clearly-identifiable R7 growth cones were traced in an approximately 10 µm-thick z-stack. Circularity was defined as: circularity = $4\pi(\text{area}/\text{perimeter}^2)$. Circularity =1 therefore indicates a perfect circle, and smaller values indicate irregular or elongated shapes.

Quantification of the frequency of R7s extending processes beyond or within their target layer. Within each brain, this frequency was determined by counting the number of R7 axon terminals exhibiting the phenotype in an approximately 10 µm-thick z-stack of the optic lobe and dividing by the total number of R7 terminals in the stack. A typical 10 µm-thick z-stack contained approximately 70 R7 terminals.

Localization of Brp-GFP puncta. We used *20C11-FLP* and the STaR technique to cause R7s to express Brp-GFP at endogenous levels. We then identified Brp-GFP puncta within R7 axons as regions that co-stained with anti-GFP and anti-Chp antibodies. This antibody staining also results in a non-specific background haze that allows optic lobe neuropil to be distinguished from cortex. We could therefore identify the medulla, lobula, and lobula plate neuropils based on position and shape (Meinertzhagen and Hanson, 1993). In R7s that overexpress Wnd, most Brp-GFP

puncta localize to the M6 layer. Within processes that Wnd-overexpressing R7s extend beyond the M6 layer, Brp-GFP puncta specifically localize to the edge of the medulla neuropil just beyond layer M10 or to a region between the lobula and lobula plate that we did not attempt to define further.

qPCR Primers. The following primer sequences (5' → 3') were used for qPCR in this study. Rpl32 Forward: CTAAGCTGTCGCACAAATGGC, Rpl32 Reverse: TTGCGCTTCTTGGAGGAGAC, Wnd Forward: GGCAGGCTAAAGAACGAGACT, Wnd Reverse: CCAAGCGGGACGGTAACAT, Faf Forward: GTGGACAGCACCATCACAATAG, and Faf Reverse: CACAAGGATACAGTGGTGGATGT

Supplementary Figures

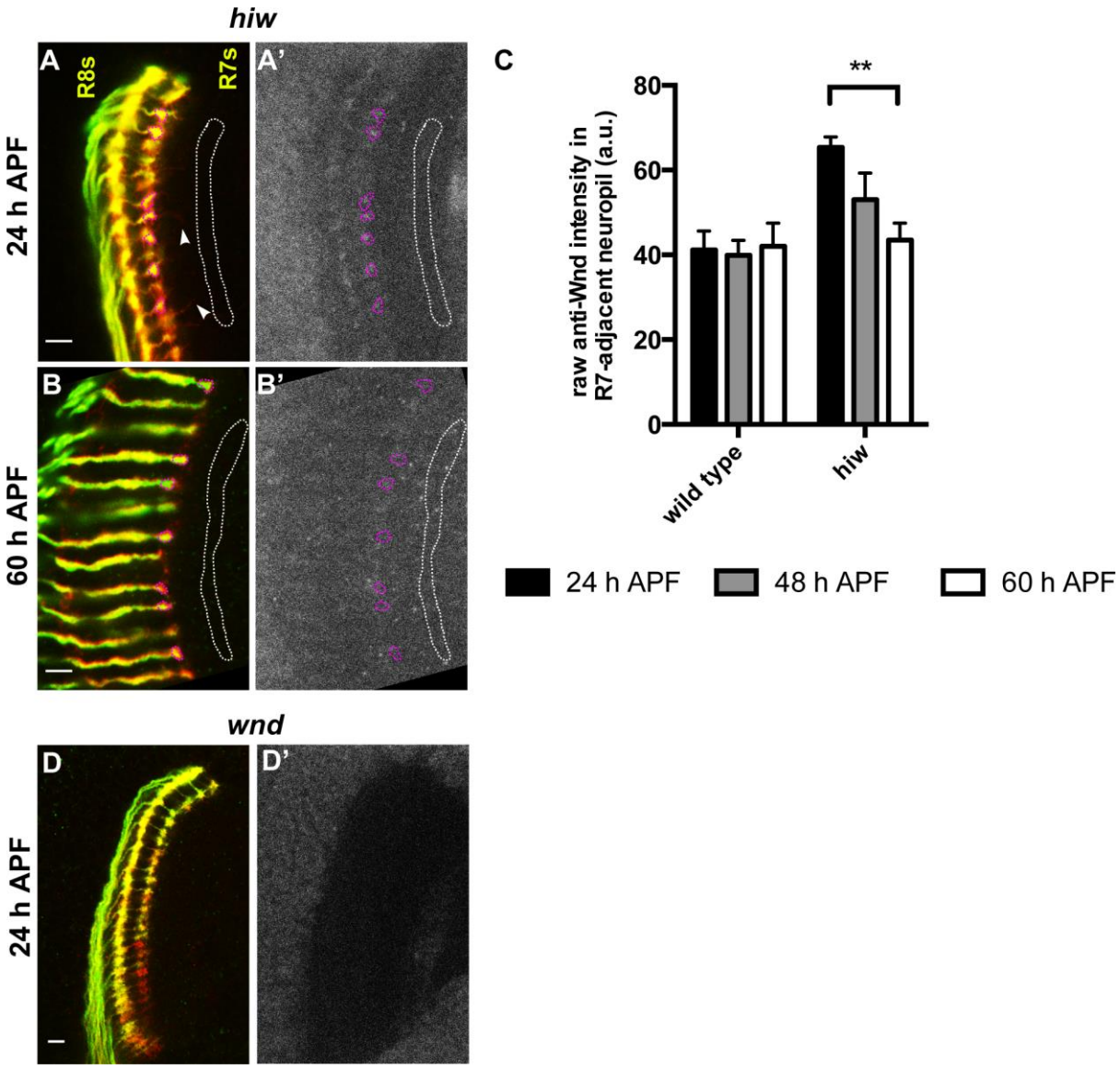

Fig. S1. Details on how anti-Wnd staining in R7 growth cones was quantified. (A-B') Exemplar *hiw* mutant pupal medullas (25°C) in which R7 and R8 are labeled with (A,B) *chp-Gal4, UAS-EB1-GFP* (green) and anti-Chp (red) and (A',B') anti-Wnd. Abnormal R7 processes are indicated by arrowheads. In all genotypes, at both 24 (A') and 60 h APF (B'), anti-Wnd staining was quantified by using anti-Chp alone to trace R7 growth cones (e.g., magenta dotted lines in A-B') and an adjacent region of neuropil (e.g., white dotted lines in A-B'). To calculate "% increase of anti-Wnd over background fluorescence" in Fig. 1E and Fig. 5A, the level of anti-Wnd staining within each R7 tracing was measured and divided by the average level of anti-Wnd staining within the adjacent region. This normalization decreased the variability caused by stochastic differences in antibody staining efficiencies among brains. (C) Quantification of average raw fluorescence intensities within the R7-adjacent

neuropil (e.g., white dotted lines in A-B') in wild-type and *hiw* mutant brains over time. n= brains, error bars represent SEM. n= 14, 19, 16, 10, 12, and 17, respectively. There is no significant change in anti-Wnd staining in this region in wild type; our use of this region to normalize the anti-Wnd staining within R7 growth cones therefore does not confer or obscure temporal differences in wild-type R7s. There is a significant decrease in anti-Wnd staining in this region in *hiw* mutant animals between 24 and 60 h APF, suggesting that a temporal, Hiw-independent mechanism might also repress Wnd in medulla axons. Our use of this region to normalize the anti-Wnd staining within *hiw* mutant R7 growth cones may therefore cause us to underestimate the strength of the Hiw-independent repression of Wnd that occurs in R7 growth cones.(D,D') *wnd* mutant pupal medulla (25°C) in which R7 and R8 are labeled with (D,E) *chp-Gal4, UAS-mCD8-GFP* (green) and anti-Chp (red) and (D') anti-Wnd. There is little anti-Wnd staining in the medulla neuropil of *wnd* protein-null mutants (quantified in Fig.1E); however, the surrounding cortex (which contains the cell bodies of medullar neurons and glia) stains brightly. We conclude that the cortical staining in this and other genotypes is therefore at least partly non-specific and does not accurately reflect Wnd levels.

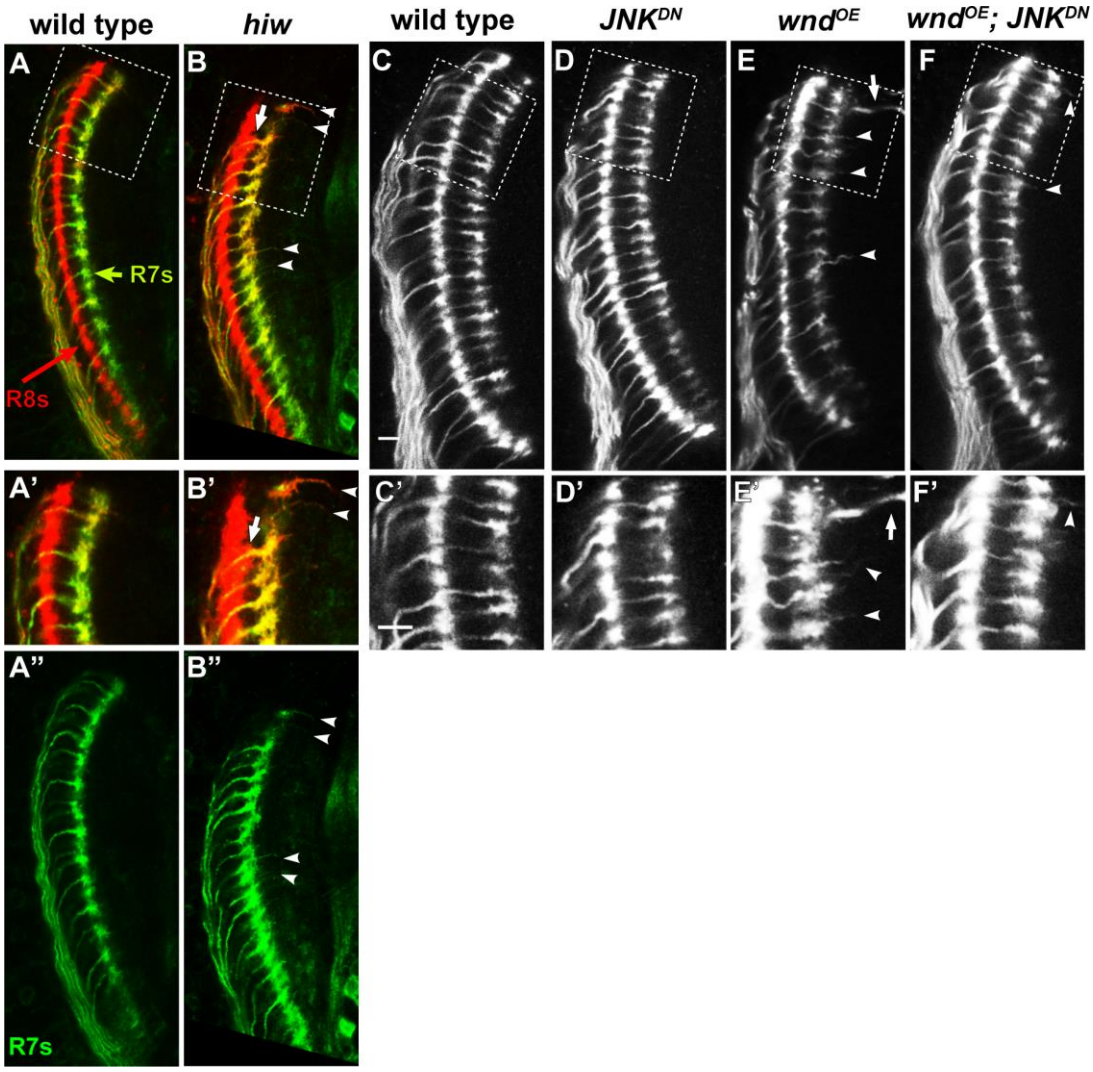

Fig. S2. Wnd disrupts layer-specific R7 growth cone halting through JNK.
(A-B") 24 h APF pupal medullas (25°C) in which R7 axons are specifically labeled with *PM181-Gal4, UAS-mCD8-GFP* (green), and both R7 and R8 axons are labeled with anti-Chp (red). A' and B' are enlargements of the boxed regions in A and B with brightness enhanced so that thin growth cone processes are visible. The R7-specific labeling confirms that it is the R7s in *hiw* mutants that extend processes beyond their target layer (arrowheads) and that it is not R7s that occasionally terminate between the R8 and R7 target layers (arrow in B and B' pointing to growth cone between R8 and R7 target layers that is stained red but not green).
(C-F'), 24 h APF pupal medullas (29ºC), in which R7 and R8 axons are labeled with *chp-Gal4, UAS-EB1-GFP* (white) . Scale bars are 5 µm. (C'-F') are enlargements of the boxed regions in (C-F) with enhanced brightness. R7 growth cones expressing dominant-negative JNK (JNK^{DN}; D,D') are indistinguishable from wild type (C,C'). R7 growth cones expressing wild-type Wnd (Wnd^{OE}; E,E') extend processes beyond their target layer (arrowheads); these processes resemble those in *hiw* mutants but sometimes extend deeper into the optic lobe (arrows). Co-expressing JNK^{DN} with wild-type Wnd almost completely ameliorates this defect (F,F', arrowheads indicate some remaining abnormal processes). These phenotypes are quantified in Fig. 2G.

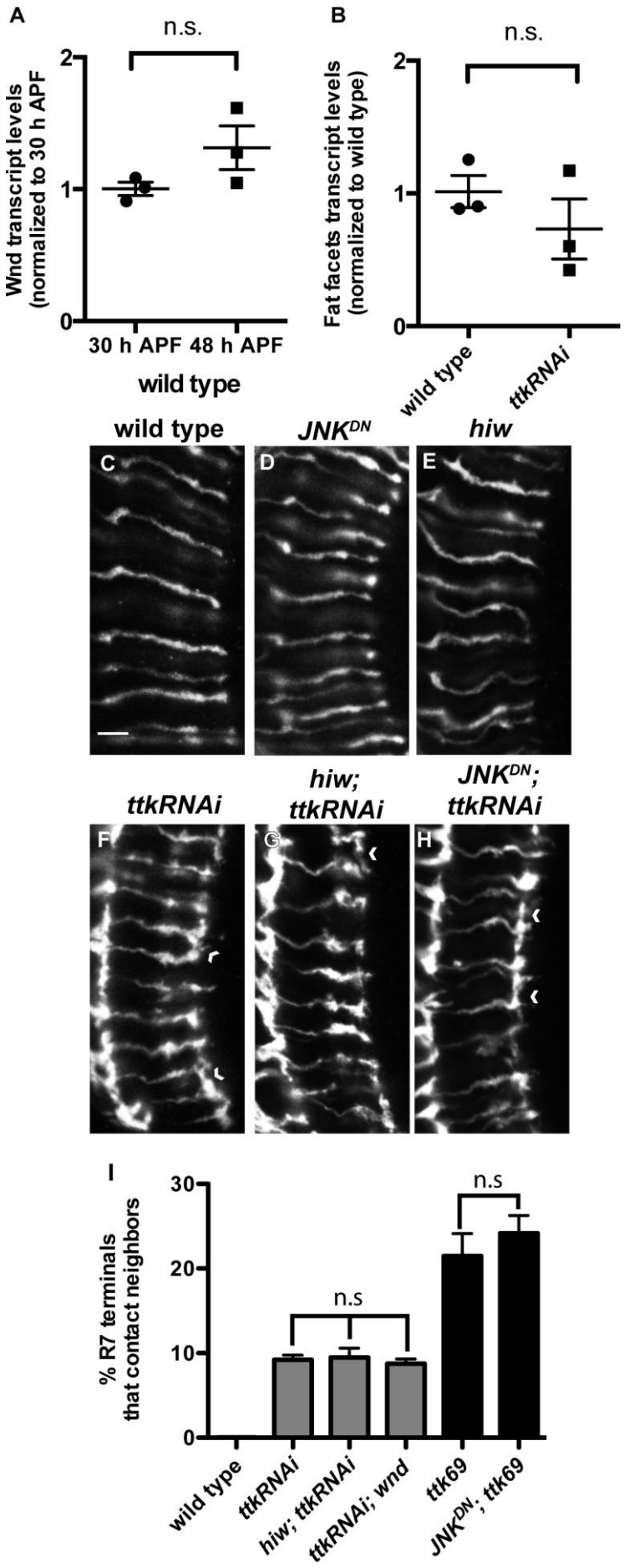

Fig. S3. Ttk69 regulates Wnd protein expression indirectly and regulates additional pathways to promote R7 growth cone remodeling.
(A,B) Quantifications of transcript levels measured by qRT-PCR on RNA extracted from dissected retinas. n= 3 biological replicates, and error bars represent SEM. (A) There is no detectable change in *wnd* mRNA levels as R7 growth cone remodeling progresses. (B) Loss of *ttk69* from R neurons does not detectably increase *fat facets* (*faf*) mRNA levels. (C-H) 48 h APF pupal medullas (29°C) in which R7 and R8 axons are labeled with *chp-Gal4, UAS-EB1-GFP*. Scale bars are 5 µm. (I) Quantification of the frequency with which R7 axon terminals contact their neighbors. n=brains and error bars represent SEM. n.s. not significant based on a pairwise two-tailed t-test. n=17, 22, 11, 10, 5, and 9, respectively. Wild-type (C), JNK^{DN}-expressing (D), and *hiw* mutant R7 axon terminals (E) are indistinguishable. The frequency with which R7s expressing *ttkRNAi* contact their neighbors (F; chevrons) is not increased by additional loss of *hiw* (G,I). And loss of *JNK* (caused by expressing JNK^{DN}; H) or *wnd* (I) from *ttkRNAi*-expressing R7s does not ameliorate this defect. Similarly, disrupting *JNK* in *GMR-FLP*-generated *ttk69* mutant R7s (by causing them to express JNK^{DN}) does not ameliorate this defect. Note that contacts between individually-labeled *GMR-FLP*-generated *ttk69* mutant R7 axon terminals and their neighbors are easier to score than contacts among uniformly labeled R7 axon terminals, so the frequency of this defect is scored as much higher in the former situation.

Multimedia

Spinning disk confocal movies, each spanning 30 minutes of real time, sped up 300x (10 frames were collected every 30 seconds but are here presented at 1 frame/second). See Methods for imaging conditions.

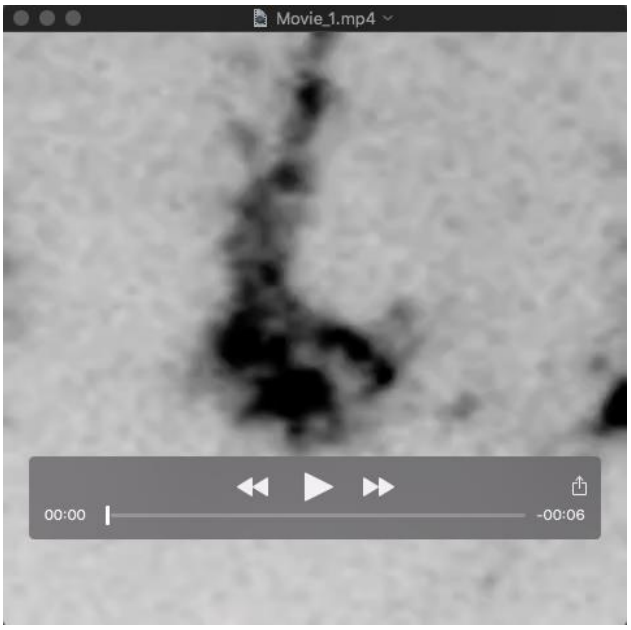

Movie 1. Representative wild-type R7 axon terminal at 40 h APF.

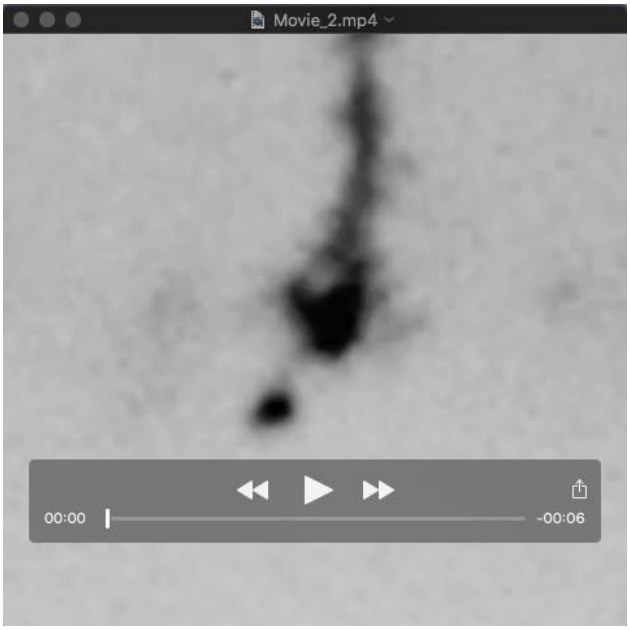

Movie 2. Representative wild-type R7 axon terminal at 48 h APF. The average extension and retraction velocities of processes are reduced compared to 40 h APF.

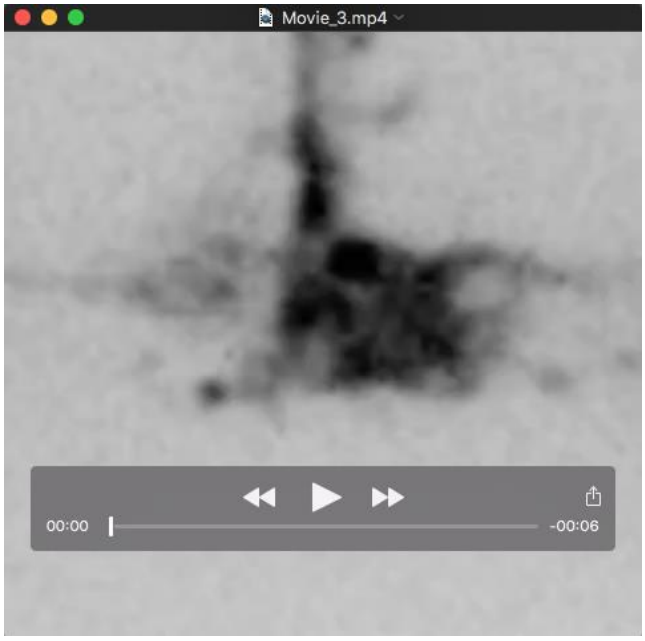

Movie 3. Representative *wnd*^{OE} R7 axon terminal at 40 h APF. The average extension and retraction velocities of processes are indistinguishable from those in wild type at 40 h APF.

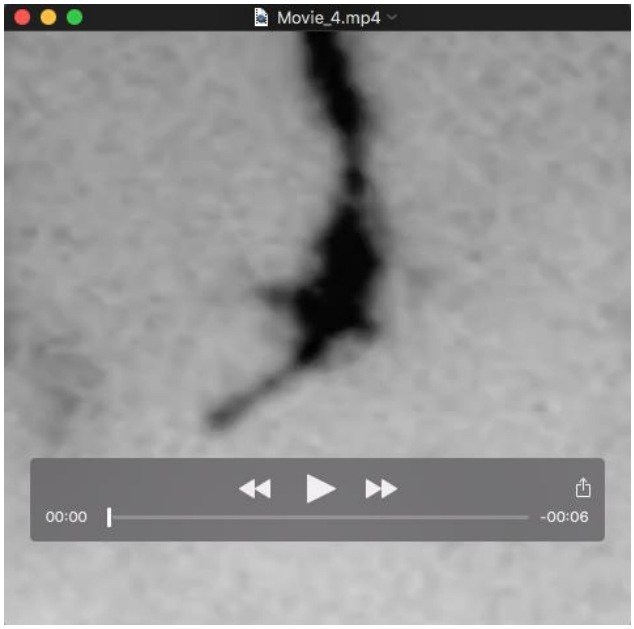

Movie 4. Representative *wnd*^{OE} R7 axon terminal at 48 h APF. The average extension and retraction velocities of processes are greater than those in wild type at 48 h APF.

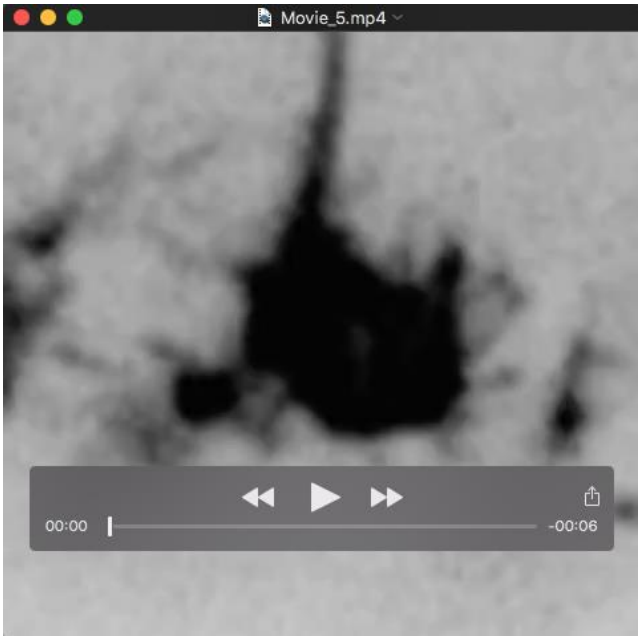

Movie 5. Representative *ttkRNAi*-expressing R7 axon terminal at 40 h APF. The average extension and retraction velocities of processes are indistinguishable from those in wild type at 40 h APF.

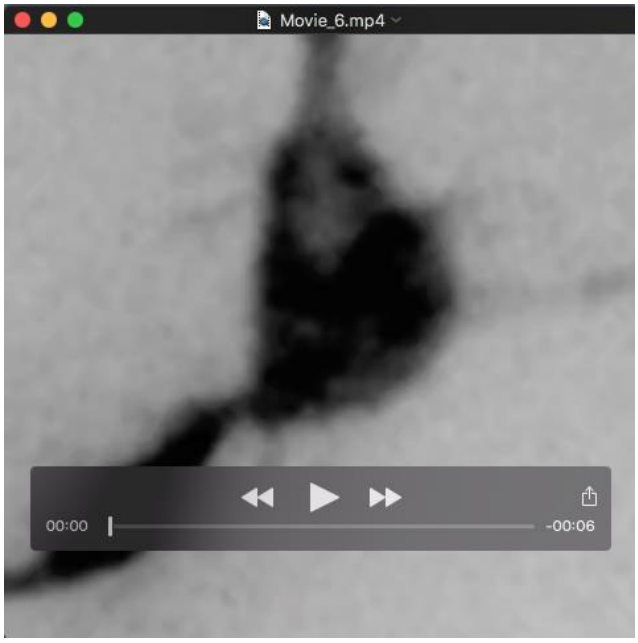

Movie 6. Representative *ttkRNAi*-expressing R7 axon terminal at 48 h APF. The average retraction velocity of processes is indistinguishable from that in wild type at 48 h APF; however, the average extension velocity of processes is greater than that in wild type at 48 h APF.